

# **Modeling Annual Energy Production of a Point Absorber Wave Energy Converter for the Great Lakes**

A THESIS

SUBMITTED TO THE FACULTY OF THE  
UNIVERSITY OF MINNESOTA DULUTH

BY:

**Khan Ahsan-Ul Muzib**

IN PARTIAL FULFILLMENT OF THE REQUIREMENTS  
FOR THE DEGREE OF  
MASTER OF SCIENCE  
IN MECHANICAL ENGINEERING

**Dr. Craig Hill**

Advisor

August 2023

© Copyright by Khan Ahsan-UI Muzib 2023

All Rights Reserved

## Acknowledgments

I extend my heartfelt gratitude to the Almighty ALLAH for the successful culmination of this research endeavor in accordance with the planned objectives.

I am profoundly indebted to my advisor, Dr. Craig Hill, whose unwavering support and guidance have been instrumental in the execution of this research project. His continuous mentorship, inspirational insights, and motivational encouragement have played an indispensable role in the realization of this work. His invaluable suggestions and constructive critique have significantly contributed to shaping the outcome. I attribute my newfound interest in renewable energy to his profound influence, which has ignited my passion for a career in this domain.

I would like to express my sincere appreciation to Dr. Craig Hill, Dr. Alison Hoxie, and Dr. Sam Toan for graciously agreeing to serve as members of my thesis committee. Their willingness to contribute their expertise and insights has enriched the quality of this research.

To my family and beloved wife, I extend my heartfelt thanks for their unwavering support throughout this transformative journey. Their encouragement and belief in my capabilities have been a wellspring of motivation.

Lastly, I am indebted to my Duluth family and the presence of Lake Superior, both of which have provided a reassuring sense of belonging and inspiration during moments when they were needed most.

## Dedication

This dissertation is dedicated to my parents, my beautiful wife, my advisor Dr. Craig Hill, and Lake Superior.

## Abstract

This project assesses the feasibility of small-scale wave energy extraction from Lake Superior, characterized by its vast expanse and high frequency wave conditions. The research aims to evaluate the power performance of a heaving-point-absorber wave energy converter (WEC) using 15 years of historical wave observation data from NDBC 45006 located in western Lake Superior. Results aim to determine the viability of deploying similar WECs in the Great Lakes region and their potential contribution to the blue economy and marine renewable energy sector.

This investigation involves the comprehensive simulation of the power generation capabilities of a point absorber WEC, specifically tailored to the wave conditions typical in western Lake Superior. To accomplish this, frequency domain modeling established WEC hydrodynamic coefficients and provided essential insights into the system's behavior in various sea states where the most common sea states were wave heights up to 1m with wave periods between 3-5 seconds, accounting for nearly 65.5% of all observations. Subsequently, through time domain analysis coupled with a hydraulic power take-off system, the WEC system's response and power output are estimated using the hydrodynamic coefficients data in the WEC-Sim software, designed to model the dynamic response of multi-body floating systems in various sea states.

The power performance of the WEC resulted in an annual average electrical power output of 6.6 MWh, showcasing the feasibility of implementing small-scale WECs in Lake Superior. Additionally, the research identifies and discusses areas that require further investigation. These findings emphasize the potential of harnessing wave energy from Lake Superior, highlighting its role in marine renewable energy development and the blue economy. This includes powering remote oceanographic sensors and observation systems, establishing AUV recharging stations, and supporting aquaculture farms. The study also underscores the importance of continued research to advance our understanding of wave energy conversion within the Great Lakes context.

# Table of Contents

Abstract.....	iii
List of Tables .....	vi
List of Figures .....	vii
Chapter 1 – Introduction.....	1
1.1 Advantages of wave energy conversion: .....	2
1.2 Challenges of wave energy conversion: .....	3
Chapter 2 – Wave Energy Converter Technologies and Industry Overview.....	5
2.1 A brief history of WECs .....	5
2.2 According to the location:.....	8
2.2.1 Shoreline Devices: .....	8
2.2.2 Nearshore Devices: .....	9
2.2.3 Offshore Devices: .....	10
2.3 According to the geometry: .....	11
2.3.1 Point Absorber: .....	12
2.4 Terminators: .....	12
2.4.1 Attenuators: .....	13
2.5 According to the working principle: .....	14
2.5.1 Oscillating Water Column (OWC) .....	14
2.5.2 Overtopping Device (OTD) .....	15
2.5.3 Wave Activated Bodies (WAB).....	15
2.6 Scaling Method for Reshaping the WEC .....	17
2.7 Selection of Suitable WEC for Shape Scaling.....	20
2.8 Research Motivation .....	24

Chapter 3 - Numerical computational methodology.....	27
3.1 Choosing the Appropriate Modeling Method.....	27
3.2 Capytaine Overview.....	28
3.3 WEC-Sim Processing.....	29
3.4 Equation of motion in time domain .....	30
Chapter 4 – Modelling and Simulation.....	35
4.1 Scaled model geometry characteristics.....	35
4.2 3D diffraction and radiation analysis methodology using Capytaine.....	37
4.3 Simulink PTO .....	38
4.4 Pre-processing in WEC-Sim using BEMIO .....	39
Chapter 5 – Results and Discussion.....	42
Chapter 6 – Conclusion.....	52
Chapter 7 - Future Recommendations .....	54
References.....	56
APPENDIX A.....	60
APPENDIX B.....	61

## List of Tables

Table 2.1: Lambda scaling factors for model testing (Martin et al., 2014). .....	17
Table 2.2: Comparing the size of different WEC categories (Babarit, 2015).....	21
Table 4.1.: Mass of the two bodies of the RM3 reference model ( <i>WEC-Sim</i> , 2022) .....	35
Table 4.2: RM3 reference model specification ( <i>WEC-Sim</i> , 2022). .....	36
Table 4.3: Mass of the two separate bodies of the scaled RM3 reference model.....	37
Table 4.4: Specifications of the scaled RM3 model. ....	37
Table 5.1: Observation counts for the NDBC 45006 sea states.....	42
Table 5.2: Joint probability distribution (JPD) for the NDBC 45006 sea states using 15 years of observations (2008-2022).....	43
Table 5.3: Electric power matrix (in kW) for the modeled RM3 WEC. ....	49
Table 5.4: Annual energy production (AEP) (MWh) for the modeled WEC. Sea states with blank boxes were not simulated in <i>WEC-Sim</i> . ....	50

## List of Figures

Figure 2.1: Power potential of marine energy resources across the United States, U.S. territories, and freely associated states (Kilcher et al., 2021). .....	6
Figure 2.2: Schematic outlining different regions where WECs may be deployed (Bouhrim & El Marjani, 2019). .....	11
Figure 2.3: Examples of different wave energy converters based on location (a) Eco wave power (2020), (b) Artists representation of Oyster device (Whittaker & Folley, 2012), (c) Pelamis P1 (Gobato et al., 2015) .....	11
Figure 2.4: Different types of WECs based on their design-(a) Image of Wave star wave energy device during normal operation, located on the Danish North Sea coast with a power rating of about 1000 kW (Marquis, 2010)., (b) Artist’s rendering of Waveroller made by AW-energy with 300 kW unit power (2022a), (c) Movement of Pelamis attenuator with 750 kW unit power (Poullikkas, 2014). .....	14
Figure 2.5: (a) Pico power plant operational principle (Rahm, 2010), (b) Overtopping device principle (Wale & Hill, 2018). .....	16
Figure 2.6: Wave energy converter classification for oscillating water column (OWC), overtopping devices (OTBs), and wave activated bodies (WABs) according to location and operating principle (Czech & Bauer, 2012). .....	16
Figure 2.7:Geographical location of NDBC buoy- (a) Buoy 45006 deployed in Lake Superior where the site is elevation of 183 m above mean sea level, (b) Buoy 46212 deployed in Humboldt Bay, CA where the site is at sea level. ....	20
Figure 2.8: Relationship between capture width ratio (CWR), characteristic diameter (CD, or width), and WEC category (Babarit, 2015). .....	22
Figure 2.9: Schematic of the two-body point absorber RM3 WEC ( <i>WEC-Sim</i> , 2022). ...	23

Figure 2.10: Marine Energy Atlas, showing the omnidirectional wave power. The yellower it gets; the more power is available at that area. The bluer it gets, the lesser power available in that area. (2022b).....	25
Figure 3.1: WEC-Sim modular structure (Yu, Lawson, et al., 2014). .....	27
Figure 3.2:Capytaine process chart.....	28
Figure 4.1: Full-scale Reference Model 3 (RM3) modified by the WEC-Sim team ( <i>WEC-Sim</i> , 2022). The yellow cylindrical feature near the top is the float. The other component of the RM3 WEC is called the spar. ....	35
Figure 4.2: CAD model and dimensions of the scaled RM3 float and spar. ....	36
Figure 4.3: Simulink model for the hydraulic PTO used during this study of the RM3. .	39
Figure 5.1 Plot illustrating the ramp up time for the hydraulic motor for a wave of 0.75m height with dominant wave period of 4.5s.....	44
Figure 5.2:Artist's representation of the hydraulic PTO system ( <i>WEC-Sim</i> , 2022).....	45
Figure 5.3: Zoomed view of the force generated the hydraulic PTO for a wave of 0.75m height with dominant wave period of 4.5s.....	46
Figure 5.4: Top and bottom piston pump pressures for a wave of 0.75m height with dominant wave period of 4.5s.....	47
Figure 5.5: Full view of the plot showing the absorbed power, mechanical power and electrical power in kW. ....	48
Figure 5.6: Detailed view of the plot showing the absorbed power, mechanical power and electrical power in kW. ....	48

## Chapter 1 – Introduction

The world is increasingly turning towards renewable energy sources in the face of mounting concerns over climate change, dwindling fossil fuel reserves, and the need for sustainable energy solutions. Among these, wave energy has emerged as a promising and untapped resource with the potential to revolutionize the global energy landscape. Harnessing the power of ocean waves, wave energy offers a clean, reliable, and abundant source of renewable electricity generation.

With approximately 71% of the Earth's surface covered by oceans, waves represent a vast and virtually inexhaustible energy reservoir. The kinetic energy of ocean waves, created by the wind's interaction with the ocean's surface, holds the key to unlocking this valuable renewable energy source. Wave energy conversion technologies, known as wave energy converters (WECs), have been designed to capture and convert this energy into usable electricity.

The concept of wave energy conversion is not new and has been explored for several decades. Several notable examples include Salter's Duck (made in 1970s) (Iphofen, 2022), the Pelamis WEC (made in 2004) (Gobato et al., 2015), the Oyster device made by Aquamarine (installed in 2009) (Whittaker & Folley, 2012), and the Waveroller device (installed in 2012) (2022a), among many other examples. However, recent advancements in technology, materials, and understanding of ocean dynamics, controls of WECs, and ability to model the dynamic response of multi-body, floating systems in these complex environments have revitalized interest in wave energy as a viable solution to address the global energy crisis and climate change. As countries seek to diversify their energy portfolios and reduce their dependence on fossil fuels, wave energy has emerged as a compelling alternative with numerous advantages. Wave energy conversion presents a promising avenue for harnessing renewable energy from vast ocean resources. It offers several advantages and, at the same time, faces various challenges that

must be addressed to realize its full potential. The following sections provide an overview of some of these advantages and challenges associated with WEC technology development.

### 1.1 Advantages of wave energy conversion:

- **Abundant and Renewable Resource:** Waves are a constant renewable energy resource, ultimately driven by solar energy and wind patterns. They are available in coastal regions worldwide, making wave energy a reliable and sustainable option for electricity generation. The estimated worldwide gross theoretical resource of power stands at approximately 3.7 terawatts (TW) (Mørk et al., 2010).
- **Predictability:** Wave energy is more predictable than some other renewable sources like wind and solar (Rusu & Soares, 2013). Advanced wave forecasting models enable accurate predictions of wave patterns, facilitating effective energy planning and grid integration (O'Donncha et al., 2018).
- **High Energy Availability:** Ocean waves have a higher energy availability than other renewable sources. While global wave energy resources has been estimated as 3.7 TW (Mørk et al., 2010), wind and solar energies are estimated to be at 900 GW (Bojek, 2023a) and 800 GW (Bojek, 2023b) respectively.
- **Low Greenhouse Gas Emissions:** Wave energy is a clean and environmentally friendly energy source. It does not produce greenhouse gas emissions during electricity generation, therefore minimizing contributions to climate change.
- **Consistent Energy Generation:** Unlike solar and wind energy, wave energy is more consistent and less affected by weather fluctuations, offering a stable and reliable power supply.
- **Integration with Different Platforms:** Wave energy projects can be strategically integrated with existing platforms, such as offshore wind turbines or oil and gas platforms, to optimize marine space utilization and reduce individual installation expenses (Pérez-Collazo & Iglesias, 2012). Moreover, these projects have the

potential for integration with expansive floating platforms, serving diverse functions such as airports, seaports, aquaculture facilities, recreational spaces, and residential areas (Nguyen et al., 2020).

## 1.2 Challenges of wave energy conversion:

- **Technological Complexity:** Developing efficient and robust WECs is a significant challenge. The harsh marine environment, including extreme weather conditions and saltwater corrosion, requires advanced engineering solutions and durable materials.
- **High Capital Costs:** The initial investment for installing and deploying wave energy systems can be substantial. It can be as much as 41% of project life cost (Kempener & Neumann, 2014). High capital costs can hinder widespread commercialization and limit the competitiveness of wave energy compared to conventional energy sources.
- **Variable Wave Resources:** Wave resources vary geographically and seasonally, affecting the energy output and project viability. Accurate wave resource assessment is critical for selecting suitable locations and optimizing system design. For instance, waves characterized by lower frequencies, such as those in ocean environments, yield greater power output compared to waves with higher frequencies, like those found across the Great Lakes. However, the energy of higher frequency waves dissipates more rapidly (Coe et al., 2021).
- **Environmental Impact:** Deploying WECs may have environmental consequences, such as altering wave patterns, disturbing marine ecosystems, and affecting marine life migration (Hildenbrand, 2014). Changes in wave pattern could also impact sediment transport and beach nourishment. Environmental impact assessments and mitigation strategies are essential to ensure sustainable development.

- **Grid Integration:** Integrating wave energy into existing electricity grids poses challenges due to wave frequency variability and matching generated electricity to grid frequencies. Additionally, similar to other renewable sources, there are challenges with storing energy produced for later use.. Smart grid technologies and energy storage solutions are required to balance supply and demand effectively (Said & Ringwood, 2021). Many developers are starting off by pursuing blue economic opportunities and advancing WEC technologies to integrate into smaller, local, non-grid power applications (LiVecchi et al., 2019).
- **Policy and Regulatory Barriers:** The nascent nature of wave energy may lead to a lack of supportive policies, incentives, and standardized regulations (Conway, 2019). Stable and favorable policies are needed to encourage investment and foster technological advancements.
- **Social Acceptance:** Public acceptance and community engagement are crucial for the success of wave energy projects (Heras-Saizarbitoria et al., 2013). Addressing concerns related to visual impacts, navigational safety, and effects on local fisheries and tourism is vital.
- **Competition with Established Energy Sources:** Wave energy faces competition from mature renewable energy sources like wind and solar. The average global levelized cost of electricity (LCOE) for new onshore wind projects stands at approximately \$0.033/kWh. Additionally, the LCOE for new utility-scale solar PV has decreased to around \$0.048/kWh, and offshore wind projects have seen a decline to about \$0.075/kWh (2021). In the realm of wave energy, the LCOE varies between \$0.35/kWh and \$0.85/kWh, with an average of \$0.57/kWh (Baca et al., 2022). To compete effectively, wave energy must prove its economic viability and scalability.

## **Chapter 2 – Wave Energy Converter Technologies and Industry Overview**

Wave Energy Converters (WECs) are innovative devices designed to harness the energy present in ocean waves and convert it into useful electricity or other forms of energy. They are part of the broader field of marine renewable energy technologies that aim to harness the vast and untapped potential of the world's oceans to produce clean and sustainable energy.

### **2.1 A brief history of WECs**

The idea of harnessing energy from the ocean has a long history, with patents for WECs dating back to 1799 (Ross, 1995). The earliest reported use of a wave energy converter was done by Y Masuda, who developed a small navigation buoy that was wave powered (Masuda, 1986). The renewed interest in wave energy research during the 1970s and 1980s was primarily motivated by the global oil crises, which highlighted the limited nature of fossil fuel reserves and the environmental impacts of using petroleum-based fuels. In recent years, pursuits of wave energy technologies have rapidly grown around the world because of a clear understanding of the power potential in the waves on our oceans and largest lakes around the world. In particular, a recent focus has emphasized how wave energy converters can contribute to a variety of blue economic industries with traditionally high cost of energy (LiVecchi et al., 2019).

Renewable energy sources, including ocean wave energy, are attractive alternatives due to their sustainability and cleaner operation. Among all renewable energy sources derived from the ocean, wave energy possesses the second-greatest capacity for energy generation (Thorpe, 1999);(Ilyas et al., 2014), only behind hydroelectricity. Ocean wave energy is recognized for its substantial potential as a renewable energy resource. Based on research, the maximum potential of ocean wave energy is estimated at approximately 30,000 TWh per year, which has the capacity to contribute up to 20% of

the global energy consumption in 2019 (Mitigation, 2011). The United States, with its extensive coastline, has a particularly good potential for ocean energy exploitation. The 50 states hold a marine energy technical resource of 2,300 TWh/yr, equivalent to 57% of their 2019 electricity generation. Pacific and Caribbean territories, as well as freely associated states, contribute an additional 4,100 TWh/yr of ocean thermal energy potential. Even utilizing a small fraction of this potential would significantly contribute to national energy needs. For example, tapping just one-tenth of the available marine energy resources in the 50 states could provide 5.7% of current electricity generation, powering 22 million homes (U.S. Energy Information Administration 2020) (Figure 2.1). Assuming capacity factors of 30% to 70%, this translates to 40 GW to 90 GW of marine energy projects (Kilcher et al., 2021). Figure 2.1 shows the power potential of marine energy resources across United States, U.S. territories, and freely associated states.

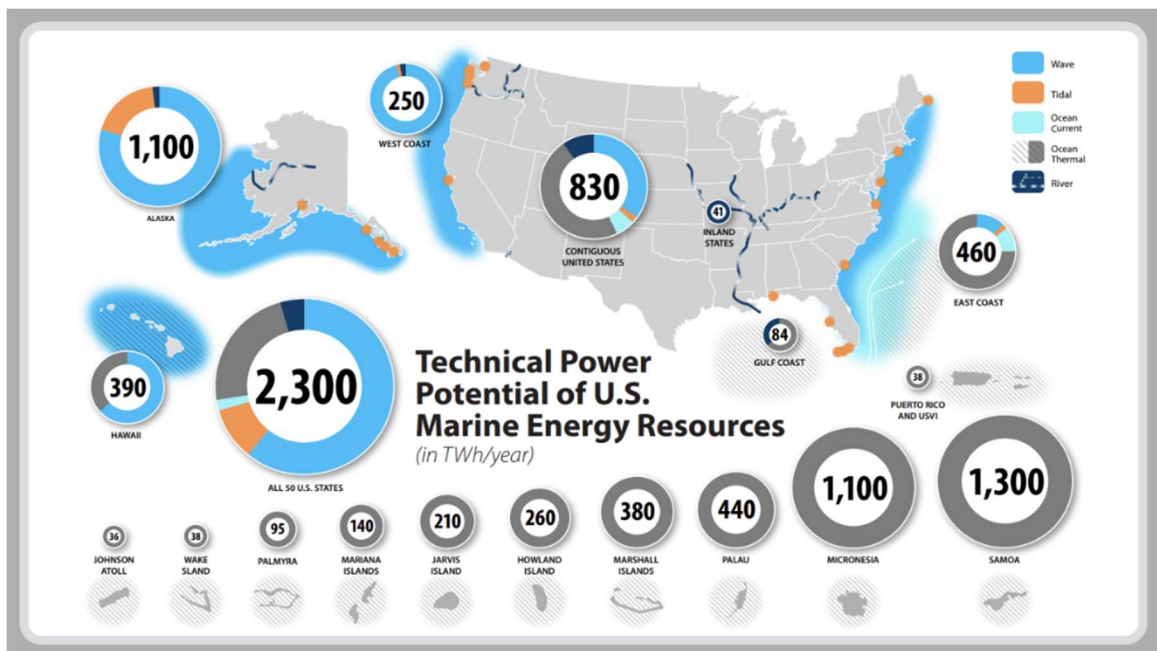


Figure 2.1: Power potential of marine energy resources across the United States, U.S. territories, and freely associated states (Kilcher et al., 2021).

The United States Department of Energy (DOE) has been actively involved in advancing the blue economy by exploring innovative ways to harness energy from the ocean, particularly through the development of marine renewable energy technologies. The DOE's efforts include research and development initiatives aimed at unlocking the potential of wave, tidal, and offshore wind energy, which can contribute significantly to both energy generation and job creation.

Based on data from the DOE's published report '*Powering the Blue Economy (PBE)*' (LiVecchi et al., 2019), five ocean observing scenarios were examined. Those are- powering coastal weather buoys at a high latitude for accurate weather forecasting, powering high frequency radar in coastal communities, powering AUV recharging stations, powering tsunami detecting stations in deep ocean, and powering drifting profilers. These cases highlight the substantial potential of marine energy to serve as a power source for diverse ocean observation platforms, sensors, and missions (Cavagnaro et al., 2020).

The development of WECs has seen numerous concepts and designs, but most of them are still in the early stages of design, laboratory testing, or prototype testing. Only a limited number of WECs have been deployed commercially due to several challenges. As previously mentioned in Section 1.2, one of the big challenges is the integration of power from large WECs into the existing electricity grid. This requires the establishment of new grid facilities in wave resource-rich areas, which adds complexity to the commercial utilization of wave energy. Similar to the European Marine Energy Center (EMEC), the US DOE is currently constructing the first grid-connected wave energy test site in the Pacific Ocean off the coast of Newport, Oregon. Other mid-scale to full-scale WEC test sites is available or in development too, such as in Hawaii, or new targeted sites off the eastern coast of the US in the Atlantic Ocean.

Various factors need to be considered in the deployment of WECs. Competing ocean use is one such factor that may limit the available space for WEC installations.

Additionally, extreme weather conditions and wave properties influenced by water depth pose technical challenges to the reliable operation of WECs. These factors require careful planning and engineering to ensure the successful implementation of large-scale commercial WECs.

While successful testing of WEC models and prototypes has been reported, upscaling these small-scale versions into large-scale commercial systems remains a significant challenge. The primary focus has been on developing large-scale converters that can efficiently contribute power to the grid. However, exploring the potential of small-scale standalone WECs to meet specific energy needs could increase their utilization and make them a valuable addition to the overall mix of renewable energy sources.

WECs operate on the principle of extracting the kinetic and potential energy contained in ocean waves as they propagate through the water. These devices employ various mechanisms to capture the wave energy, which is then converted into mechanical or hydraulic motion. This motion is subsequently transformed into electrical energy through power take-off (PTO) systems, which are essential components of WECs.

There are different types of WECs, and they can be classified based on their location, geometry, and working principle.

## **2.2 According to the location:**

Wave energy converters (WECs) can be systematically categorized based on their spatial relationship with the sea coastline (Figure 2.2). The classification is as follows:

### **2.2.1 Shoreline Devices:**

As the name suggests, shoreline devices are wave energy converters installed in shallow water depths close to the coast or attached to manmade constructions such as breakwaters. Due to their proximity to the shore, these devices offer certain advantages,

such as being relatively easy to install and maintain. Another benefit is that they do not require long submarine power cables to connect to the power grid, simplifying and removing expense from the power transmission process. Another advantage is that since these devices are fixed to the sea bottom or manmade shoreline structures, there is no need for complex mooring systems. However, it is essential to acknowledge that shallow waters' wave power density is generally lower than deeper sea areas because wave energy dissipation through seabed friction leads to the attenuation of waves in shallow water depths. As a result, the power production capacity of shoreline devices may be limited, and they may not be able to harness as much wave energy as devices installed in deeper waters. They also have to operate in breaking wave environments, which adds new challenges.

Vertical and horizontal oscillating water column (OWC) and overtopping devices (OTD) are typically reserved for shoreline installations. Eco wave power grid connected wave energy array is a great example of a shoreline device (Figure 2.3 (a)). Eco Wave Power's technology involves floating buoyant structures that move up and down with the motion of the waves. They have projects and installations worldwide, with their wave energy converters deployed in several countries. As of now, the company has projects in Europe, Asia, and the Americas, contributing to the global distribution of wave energy with a total power output of 262.7 MW in 2020 (2020).

### **2.2.2 Nearshore Devices:**

Nearshore devices are installed in water depths ranging from 10 to 25 meters at a distance of approximately 0.5 km to 2 km from the shoreline. These devices are often bottom-mounted, which eliminates the need for mooring systems, further simplifying their installation process. Nearshore devices have the advantage of being strategically positioned to capture a substantial portion of the wave energy as waves propagate toward the coast. They can efficiently harness the energy possessed by waves in this moderate water depth range. Most wave energy converters like OWCs, OTDs, wave activated

bodies and Oscillating surge wave energy converter (OSWEC) can be deployed nearshore. Figure 2.3 (b) shows a near-shore device called Oyster developed by Aquamarine Power. The Oyster device is a wave energy converter developed by Queen's University, Belfast (Whittaker & Folley, 2012). The Oyster device consists of a buoyant, hinged flap that moves with the motion of the waves. The movement of the flap activates a hydraulic system, which drives a high-pressure fluid to an onshore turbine, generating electricity (Whittaker & Folley, 2012).

### **2.2.3 Offshore Devices:**

Offshore devices represent a class of wave energy converters installed several kilometers away from the shore, in deep waters with a water depth exceeding 40 meters. These devices can be either floating on the water surface or submerged and moored to the sea floor. The vast wave energy potential in deep seas makes offshore devices highly attractive for wave energy conversion, as they have access to abundant wave energy resources if appropriately designed. However, installing and maintaining offshore devices presents significant challenges. Their remote locations and deep water depths make deployment and maintenance more complex and costly compared to nearshore or shoreline devices. Ensuring the survivability of these devices in extreme sea conditions is a major design challenge, requiring robust engineering solutions. Additionally, the maintenance of the long submarine cables used to connect offshore WECs to the power

grid can be a logistical challenge. Pelamis P1 is the world’s first offshore wave energy converter (Figure 2.3 (c))

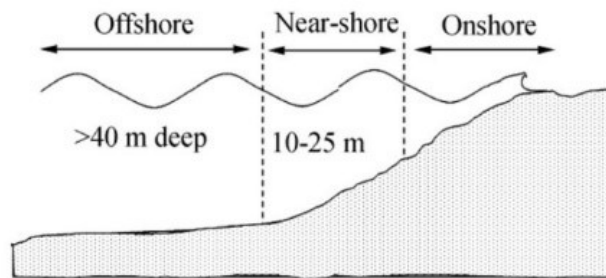


Figure 2.2: Schematic outlining different regions where WECs may be deployed (Bouhrim & El Marjani, 2019).

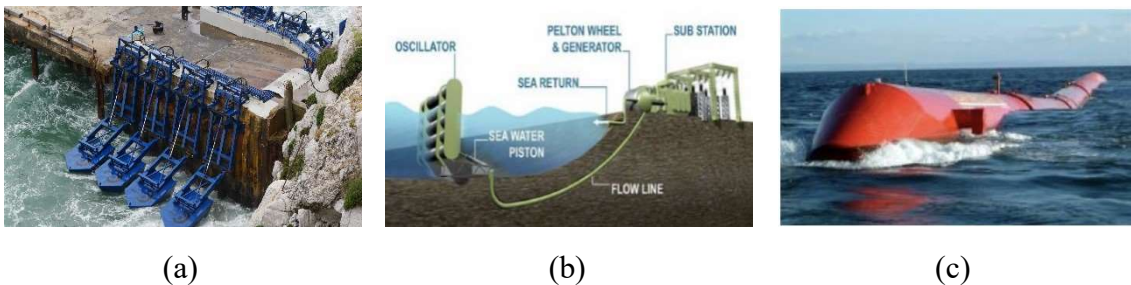


Figure 2.3: Examples of different wave energy converters based on location (a) Eco wave power (2020), (b) Artists representation of Oyster device (Whittaker & Folley, 2012), (c) Pelamis P1 (Gobato et al., 2015)

### 2.3 According to the geometry:

Wave Energy Converters (WECs) can be classified based on their geometry, which determines their shape and orientation with respect to wave propagation. This classification provides valuable insights into the design and operational characteristics of

different types of WECs. Three major categories based on the geometry are discussed below:

### **2.3.1 Point Absorber:**

The point absorber is typically an axisymmetric oscillatory device that can either float on the water surface or be submerged just below the surface. Its principal dimensions are relatively small compared to the wavelength of ocean waves. The distinguishing feature of the point absorber is its ability to absorb energy from incident waves arriving from all directions, making wave direction characteristics irrelevant as a design parameter for optimizing its performance. Point absorbers are capable of harnessing energy from waves with small amplitude and short periods, and they can be installed at various water depths. While the energy absorption rate of point absorbers may be comparatively low, their performance is deemed satisfactory when considering the size and efficiency of the device. Numerous prototypes of point absorber devices have been developed, showcasing their versatility and potential for wave energy conversion. Wave star (Figure 2.4(a)) is a heaving point absorber wave energy converter device developed by Wave star Energy A/S. It is designed as a floating platform with multiple arms that move with the motion of waves. The movement of the arms drives hydraulic pumps, which then generate electricity. The device is designed to be scalable, and multiple units can be connected to form a wave farm, increasing the overall power output. The estimated power output of this WEC is about 1000 kW (Marquis, 2010).

### **2.4 Terminators:**

Terminators are long, floating WECs with their principal axis perpendicular to the direction of wave propagation. As a result, their main axis aligns parallel to the wave crests, leading to the termination of incident waves. Unlike point absorbers, terminators have horizontal dimensions comparable to or larger than the incident wavelengths.

Consequently, they absorb energy in only one direction, making them suitable for onshore or nearshore locations.

Terminators typically consist of two components: a stationary part, moored to the seafloor or shore, and a moving component that responds to wave-induced motion by moving up and down. This movement allows the terminator to capture wave energy efficiently. While onshore or nearshore installations are common for terminators, floating versions have been developed for offshore applications as well. An example of a typical terminator is WaveRoller, as shown in Figure 2.4 (b). The Waveroller device consists of a partially submerged chamber filled with seawater, and as waves enter the chamber, they cause the water level to rise and fall, creating pressure variations. These pressure variations drive air through a turbine, generating electricity. The estimated power output of the Waveroller device is around 350-400 kilowatts (2022a).

#### **2.4.1 Attenuators:**

Attenuators are horizontally large, multiple-segment, floating WECs with their principal axis aligned parallel to the direction of wave propagation. Unlike terminators, attenuators have lower areas perpendicular to the waves, which results in them experiencing reduced forces from the waves. The device is moored to the seabed, allowing it to self-align to incoming waves for optimal energy capture.

The power take-off system of an attenuator extracts power from the wave-induced motion of its hinged joints and converts it into electricity, which is then transferred to the grid. Figure 2.4 (c) illustrates an example of an attenuator's movement.

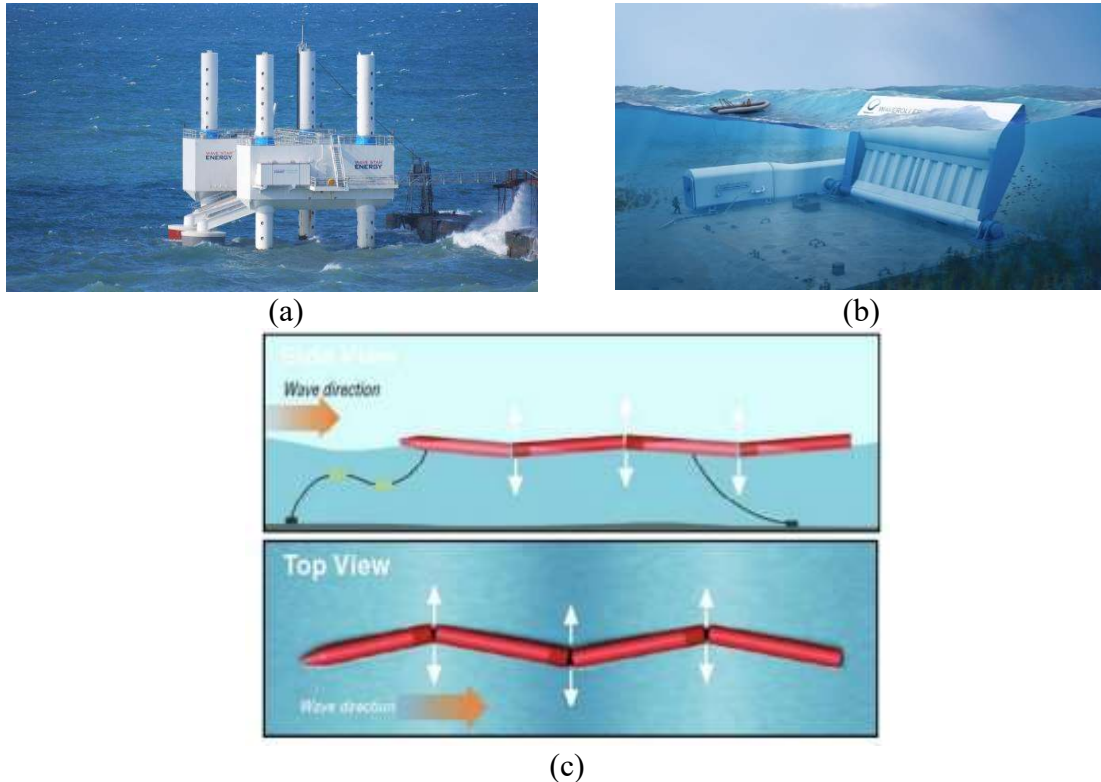


Figure 2.4: Different types of WECs based on their design-(a) Image of Wave star wave energy device during normal operation, located on the Danish North Sea coast with a power rating of about 1000 kW (Marquis, 2010)., (b) Artist's rendering of Waveroller made by AW-energy with 300 kW unit power (2022a), (c) Movement of Pelamis attenuator with 750 kW unit power (Poullikkas, 2014).

## 2.5 According to the working principle:

### 2.5.1 Oscillating Water Column (OWC)

The Oscillating Water Column (OWC) is an indirect wave energy conversion system that harnesses wave energy by converting it to air pressure. The OWC consists of a partially submerged chamber that is filled with seawater and air. As waves enter the chamber through an underwater opening to the sea, the water column rises and falls, creating a piston-like effect that compresses or extends the air inside the chamber. This oscillation of air pressure is used to actuate an air-driven turbine, which generates

electricity. The OWC system can be located either on the coastline (onshore) or on a floating platform (offshore). A well-known example of an onshore OWC is the Pico power plant system, as shown in Figure 2.5 (a).

### **2.5.2 Overtopping Device (OTD)**

Overtopping devices capture the energy of incident waves by physically capturing them and directing the water to fill a reservoir positioned above the average ocean level. The high-pressure water in the reservoir is then released back into the ocean due to gravity, passing through low-head turbines, and the energy of the trapped water is harnessed to generate electricity. Overtopping devices can be installed as fixed or floating platforms that are moored to the seabed. Unlike other WECs that rely on wave kinetic energy, these devices utilize the potential energy of the elevated water level to generate power. Figure 2. 5 (b) illustrates the wave overtopping device, showcasing its ramp design to receive incoming waves at their maximum height efficiently.

### **2.5.3 Wave Activated Bodies (WAB)**

Wave Activated Bodies (WAB) are also referred to as oscillating body systems. These devices extract energy from ocean waves by utilizing the wave-activated oscillatory motions of various body parts of the device relative to each other or relative to a fixed reference. The principal motion of floating bodies in WAB systems can be primarily described as heave, pitch, and roll. Examples of WAB devices include point absorbers, attenuators, and terminators. The motion of these bodies in response to the waves generates the necessary mechanical energy that can be converted into electrical power. Figure 2.6 provides a comprehensive illustration of the classification of WECs based on their location and operating principles.

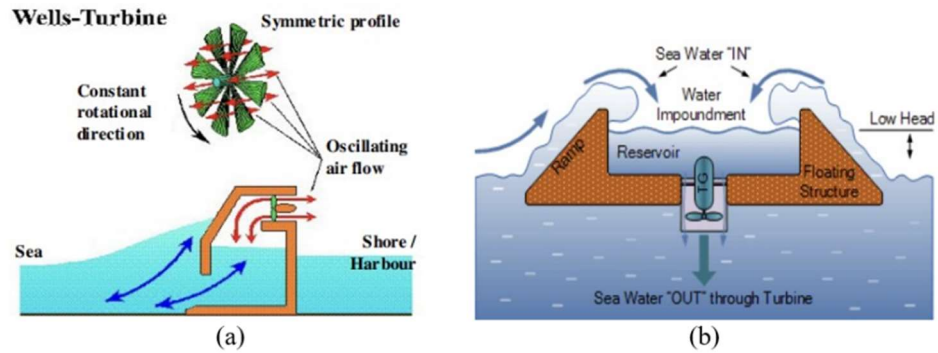


Figure 2.5: (a) Pico power plant operational principle (Rahm, 2010), (b) Overtopping device principle (Wale & Hill, 2018).

In addition to the above classification based on the working principle of the device, WECs can also be categorized according to the types of power take-off (PTO) systems used. The most common types of PTO systems in WECs include air turbines, linear generators, and hydraulic systems.

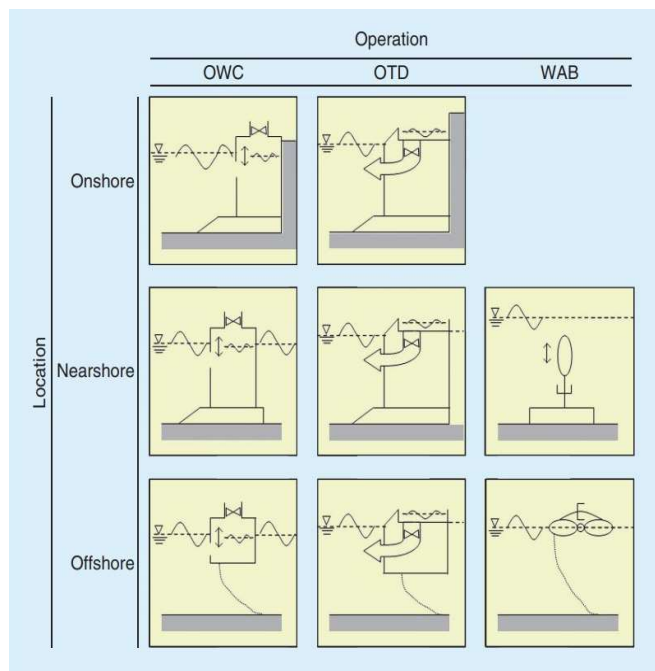


Figure 2.6: Wave energy converter classification for oscillating water column (OWC), overtopping devices (OTBs), and wave activated bodies (WABs) according to location and operating principle (Czech & Bauer, 2012).

## 2.6 Scaling Method for Reshaping the WEC

The WEC-Sim GitHub repository includes two reference wave energy converters (WECs) for analysis. One of them is the RM3 model, while the other is the OSWEC model (RM5). In order to assess the energy production of these models, reference site wave statistics were utilized. This reference site, located in Humboldt Bay, CA, was determined based on measurements obtained from a nearby National Data Buoy Center buoy (#46212) (Yu, Li, et al., 2014).

To optimize the WEC models for this research, Froude scaling was implemented. Froude scaling allows for the adjustment of physical parameters by considering the ratio of characteristic lengths between the scaled model and the full-scale device. This scaling factor, denoted as  $\lambda$ , is known as the Froude scaling factor. Table 2.1 provides the necessary factors for scaling important physical parameters based on  $\lambda$ .

$$\lambda = \frac{l_{full\ scale}}{l_{model\ scale}}$$

2.1

Table 2.1: Lambda scaling factors for model testing (Martin et al., 2014).

Parameter	Scale Factor
Length (e.g., displacement, wave height)	$\lambda$
Area	$\lambda^2$
Volume	$\lambda^3$
Angle	1
Density	1
Mass	$\lambda^3$
Time (e.g., wave period)	$\lambda^{0.5}$
Frequency (e.g., rotor rotational speed)	$\lambda^{-0.5}$
Velocity (e.g., wind speed, wave celerity)	$\lambda^{0.5}$
Acceleration	1
Force (e.g., wind, wave, structural)	$\lambda^3$
Moment (e.g., structural, rotor torque)	$\lambda^4$
Power	$\lambda^{3.5}$
Young's modulus	$\lambda$
Stress	$\lambda$
Mass moment of inertia	$\lambda^5$
Area moment of inertia	$\lambda^4$

Froude scaling is a fundamental concept in the field of wave energy converter (WEC) modeling, which plays a crucial role in understanding and predicting the performance of these devices. It allows for the accurate representation of physical phenomena observed at different scales, enabling researchers to extrapolate experimental results to larger or smaller WEC designs. In this extensive discussion, we will delve into the principles of Froude scaling, its applications in WEC modeling, and its significance in advancing wave energy technology.

Froude scaling is based on the Froude number, a dimensionless parameter used to characterize the flow behavior of waves and their interaction with structures. The Froude number ( $Fr$ ) is defined as the ratio of the wave speed ( $V$ ) to the square root of the product of the acceleration due to gravity ( $g$ ) and a characteristic length ( $L$ ). It is expressed as-

$$Fr = \frac{V}{\sqrt{g * L}}$$

2.2

By maintaining similarity in the Froude number, the wave kinematic and dynamic properties can be preserved when scaling a WEC model. When developing a physical model of a WEC, it is often impractical or cost-prohibitive to construct a full-scale prototype. Instead, researchers employ scaled-down models that exhibit similar hydrodynamic behavior to the actual device. Froude scaling provides a framework for accurately representing the behavior of waves and their interaction with the WEC at a reduced scale. By ensuring that the Froude number remains constant between the scaled model and the full-scale device, the dynamic response of the WEC can be accurately predicted.

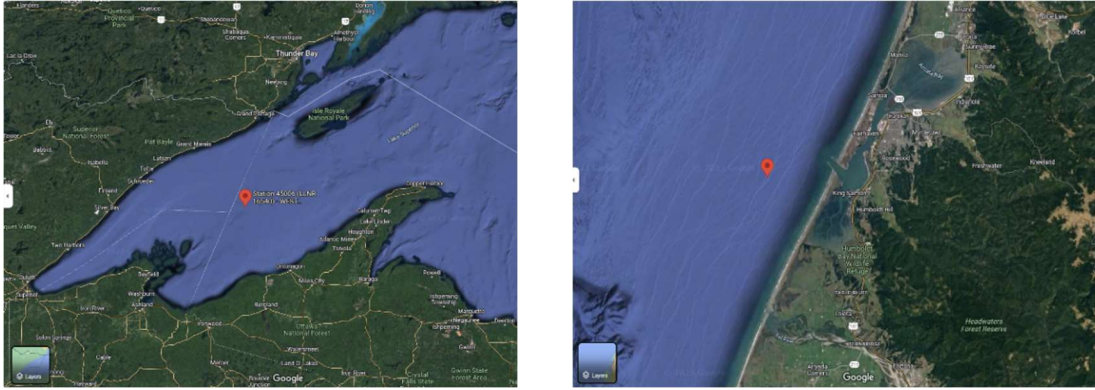
The principle of Froude scaling is particularly relevant in modeling the hydrodynamic performance of WECs, including power absorption, motion characteristics, and wave-structure interactions. Scaling laws derived from Froude scaling theory enable researchers to determine the appropriate scaling factors for physical parameters such as wave height, wave period, device size, and power extraction

efficiency. By maintaining the same Froude number, the scaled model can accurately simulate the behavior of the full-scale WEC, providing valuable insights into its performance (Khedkar et al., 2021).

Furthermore, Froude scaling allows for the extrapolation of experimental data obtained from laboratory tests to predict the performance of larger-scale WECs in real-world conditions (Sheng et al., 2014). This helps in the design optimization and cost-effective development of wave energy devices. By understanding the scaling relationships between different parameters, researchers can estimate the power output, structural loads, and other critical factors of full-scale WECs based on scaled-down model testing.

One important consideration in Froude scaling is the requirement for the scaling laws to account for both the hydrodynamic and structural aspects of the WEC. While maintaining the Froude number ensures similarity in the hydrodynamic behavior, it is essential to also consider the scaling of structural components, material properties, and device dynamics.

Data from a National Data Buoy Center (NDBC) buoy deployed in Lake Superior, West Superior- 30NM NE of Outer Island, WI (47°20'5" N 89°47'34" W) (Figure 2.7 (a)) (#45006) and buoy #46212 deployed in Humboldt Bay South Spit, CA (40°45'12" N 124°18'48" W) (Figure 2.7 (b)) were compared to determine the scaling factor. The scaling factor was found to be 1/3rd of the reference model, indicating that the scaled model utilized in this research was one-third the size of the full-scale device. This scaling factor was employed to ensure the accurate representation of the WECs in the analysis and optimization processes.



(a) (b)  
 Figure 2.7: Geographical location of NDBC buoy- (a) Buoy 45006 deployed in Lake Superior where the site is elevation of 183 m above mean sea level, (b) Buoy 46212 deployed in Humboldt Bay, CA where the site is at sea level.

## 2.7 Selection of Suitable WEC for Shape Scaling

Over the past few decades, wave energy has emerged as a prominent field of research and development in harnessing the potential of ocean energy. The wave energy converter (WEC) industry has proposed various technologies, broadly classified into OWCs and variants, overtopping devices and variants, heaving devices and variants, fixed OWSC and variants, and floating OWSC and variants based on their underlying principles of operation. To facilitate meaningful comparisons, the annual average of the Capture Width Ratio (CWR) is used as a common performance measure. CWR represents the ratio of absorbed wave power ( $P$ ) in kilowatts (kW) to the wave resource ( $J$ ) in kilowatts per meter (kW/m), providing insights into energy absorption efficiency.

$$C = \frac{P}{J} \tag{2.3}$$

While capture width offers valuable insights, hydrodynamic efficiency is a more comprehensive measure of a WEC's overall performance. Hydrodynamic efficiency, denoted as  $\eta_1$ , is calculated by dividing the capture width by the characteristic dimension

(CD) of the WEC, typically its width (B). CWR is the percentage of wave power that the device successfully absorbed.

$$\eta_1 = \frac{CW}{B} = \frac{P}{JB}$$

2.4

CWR mainly focuses on hydrodynamic power production rather than the cost of energy. Factors such as power take-off system efficiency, power conversion chain, fabrication costs, and operation costs can influence the overall efficiency of a device in terms of the cost of energy. Therefore, a WEC that excels hydrodynamically may not necessarily be the most efficient in terms of energy cost.

Statistical analysis of 90 measurements of CWR revealed fixed OWSCs as the most efficient category with an average CWR of 37%, followed by OWCs at 29%, overtopping devices at 17%, heaving devices at 16%, and floating OWSCs at 12%. Standard deviations of CWR were significant, indicating variations in power performance within each device category.

From Table 2.2 heaving devices were found to have the smallest characteristic dimensions (mean of 12 meters), followed by fixed OWSCs (mean of 18 meters) and OWCs (mean of 20 meters). Floating OWSCs and large overtopping devices had larger characteristic dimensions, with means of 33 meters and 124 meters, respectively.

Table 2.2: Comparing the size of different WEC categories (Babarit, 2015)

		OWSc	Overtopping Devices	Heaving Devices	Fixed OWSCs	Floating OWSCs
Capture width ratio (%)	Mean	29	17	16	37	12
	STD	13	8	10	20	5
Characteristic Dimension (m)	Mean	20	124	12	18	33
	STD	10	107	7	14	24

Figure 2.8 illustrates the relationship between CWR, characteristic dimension (CD), and WEC category, revealing trends such as fixed OWSCs being more efficient

and overtopping devices being less efficient in terms of wave energy absorption while heaving devices reside in between.

Among these technologies, the point absorber has garnered significant attention from researchers due to its perceived cost-effectiveness in extracting wave energy. They are also suitable to be installed in various depths of water. Modeling and analysis of point absorbers have been a focal point of many studies in the pursuit of optimizing wave energy conversion. For this research, a two-body point absorber WEC has been chosen for this study to explore energy generation potential from the Great Lakes.

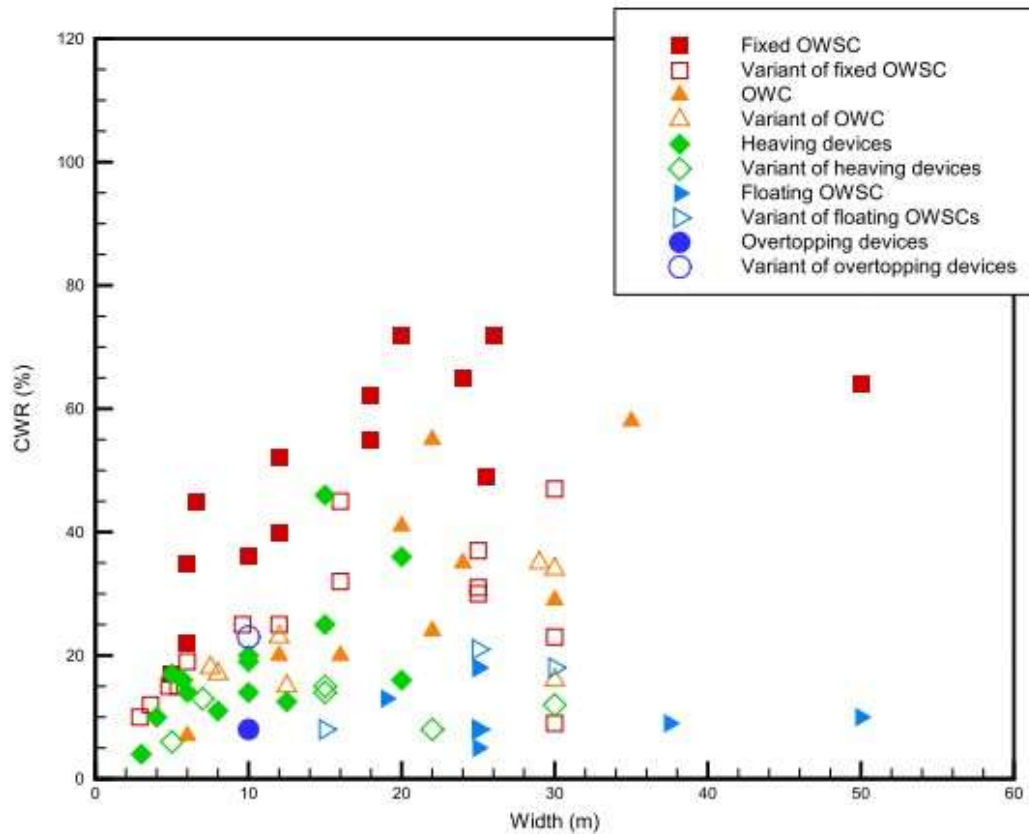


Figure 2.8: Relationship between capture width ratio (CWR), characteristic diameter (CD, or width), and WEC category (Babarit, 2015).

The point absorber that has been chosen for this research as a reference is called the Reference Model 3 (RM3) (Figure 2.9) two-body point absorber WEC. The RM3 two-body point absorber wave energy converter (WEC) has undergone comprehensive characterization through numerical simulations and experimental testing facilitated by the funding received from the Department of Energy (DOE) for the Reference Model Project (RMP) (Neary et al., 2014).

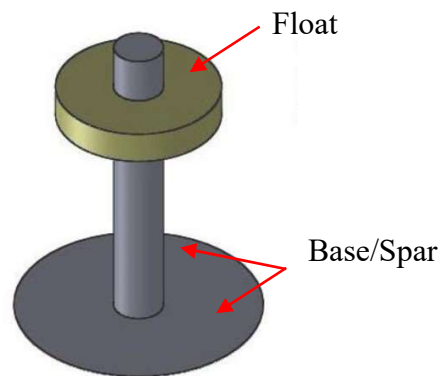


Figure 2.9: Schematic of the two-body point absorber RM3 WEC (*WEC-Sim*, 2022).

The Reference Model Project (RMP) was a significant collaborative initiative supported by the U.S. Department of Energy (DOE) that aimed to advance the development of standardized marine hydrokinetic (MHK) point designs, commonly known as reference models (RMs). The primary objective of the RMP was two-fold: First, to establish benchmarks for the performance and costs of various MHK technologies, and second, to create an open-source methodology that would facilitate the design and analysis of these technologies.

One of the key challenges faced by the MHK industry was the lack of standardized designs and performance metrics, making it difficult to compare and evaluate different technologies on a level playing field. The RMP sought to address this challenge by developing a set of reference models that could serve as standardized

benchmarks for MHK systems. These reference models were based on real-world data and performance metrics, making them reliable and relevant for the industry.

In addition to creating reference models, the RMP also aimed to establish an open-source methodology that would allow researchers and developers to design and analyze MHK technologies more efficiently. The RMP encouraged collaboration and knowledge-sharing within the MHK community by providing an open-source platform, fostering innovation and progress in the field.

To achieve its goals, the RMP project team consisted of experts and researchers from various institutions, including Sandia National Laboratories (SNL), the National Renewable Energy Laboratory (NREL), the Pacific Northwest National Laboratory (PNNL), the Oak Ridge National Laboratory (ORNL), the Applied Research Laboratory of Penn State University, and Re Vision Consulting, among various other university research labs that contributed efforts to various stages of the projects. This multi-institutional collaboration brought together diverse expertise and resources, enabling a comprehensive and robust approach to developing the reference models and methodology.

## **2.8 Research Motivation**

In an evolving energy landscape, WECs have traditionally targeted serving large-scale power generation, but a paradigm shift is underway towards their application as standalone systems for observation and offshore structures with reduced energy demands. This research is driven by the need to understand the viability of small-scale WECs across diverse and lower wave energy resource availability locations, including the Great Lakes, Gulf of Mexico, Mediterranean, and Polar regions, among others, to unlock untapped energy reserves while advancing sustainable energy sources.

The Marine Energy Atlas (Figure 2.10), a pivotal tool developed by NREL, holds insights into marine and hydrokinetic resource potential. While coastal areas have seen

wave energy assessments, the Great Lakes remain unexplored territory, hindering a comprehensive understanding of their energy potential. The significance of these energy reserves underscores the necessity to investigate how wave energy converters can harness this untapped resource, aligning with resource assessment and WEC deployment strategies.

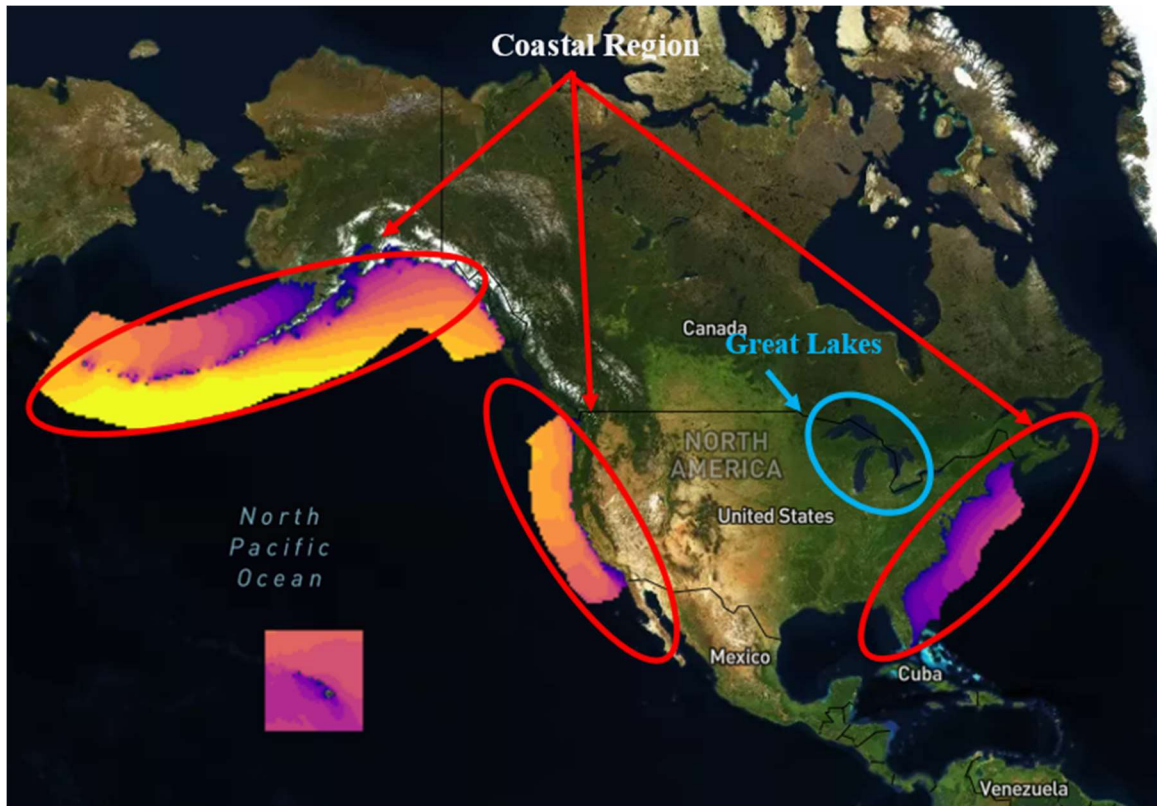


Figure 2.10: Marine Energy Atlas, showing the omnidirectional wave power. The yellower it gets; the more power is available at that area. The bluer it gets, the lesser power available in that area. (2022b).

As the 'Powering the Blue Economy' (LiVecchi et al., 2019) concept gains momentum, WECs are poised to support autonomous power demand in ocean and large lake environments. This niche application includes powering remote sensors, autonomous vehicle recharging, aquaculture farms, and many other emerging applications. Smaller-

scale WECs are gaining traction due to their ability to supply power in lower power demand scenarios, simplified deployment, and heightened capacity factors (Coe et al., 2021).

Through modeling a small-scale wave energy converter and utilizing Lake Superior wave data as input, this project aims to calculate the power performance of a heaving point absorber WEC using WEC-Sim, a software tool developed by the US National Labs to simulate dynamic motions of multi-body systems in marine environments. The broader objective is to evaluate the feasibility of integrating small-scale WECs into the Great Lakes' environment for contributing to marine renewable energy endeavors and better understand how the Great Lakes wave climate can advance WEC development and explore new opportunities to power blue economic applications. By addressing the potential of these compact energy solutions, this research aligns with the goals of sustainable energy utilization and blue economy enhancement.

# Chapter 3 - Numerical computational methodology

## 3.1 Choosing the Appropriate Modeling Method

This research utilizes time domain numerical modeling and simulation techniques to evaluate the power performance of a wave energy converter (WEC) under various design parameter combinations. The Wave Energy Converter Simulator (WEC-Sim), a specialized time domain modeling tool, is employed to predict the power generation capabilities of the WEC system.

To begin the analysis, the core hydrodynamic coefficients of the WEC are estimated using a frequency-domain boundary element method (BEM) solver with linear potential flow assumptions, specifically the Capytaine software (*Capytaine, Github Repository, 2021*). These estimated hydrodynamic coefficients serve as inputs to determine the dynamic responses and power output of the WEC system.

By integrating the time domain numerical modeling approach with the capabilities of WEC-Sim and the estimation of hydrodynamic coefficients, this study aims to provide a comprehensive understanding of the power performance of the WEC system and assess

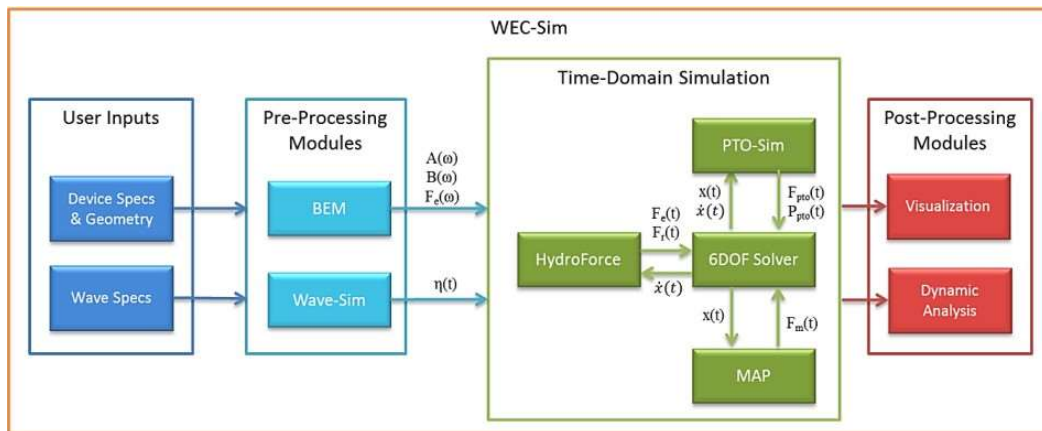


Figure 3.1: WEC-Sim modular structure (Yu, Lawson, et al., 2014).

its feasibility and potential for practical application in harnessing wave energy. The modular structure of WEC-Sim follows Figure 3.1.

### 3.2 Capytaine Overview

Capytaine is a Python-based software package designed for frequency domain simulations of the interaction between floating bodies and water waves. It is a complete rewrite of the open-source Nemoh solver, employing the linear potential flow wave theory within the Boundary Element Method (BEM). The key components of Capytaine include the Mesh, representing the geometric structure of the floating body; DOF, representing degrees of freedom for body motion; FloatingBody, combining Mesh and degrees of freedom; LinearPotentialFlowProblem, defining the problem instance with relevant parameters; Solver, the core of the code performing computations; and LinearPotentialFlowResult, storing simulation outcomes, including added masses, radiation damping, and forces. Capytaine serves as a powerful tool for analyzing and predicting various physical properties and behaviors in the interaction between water waves and floating bodies. The sequence of actions performed by Capytaine is illustrated in Figure 3.2.

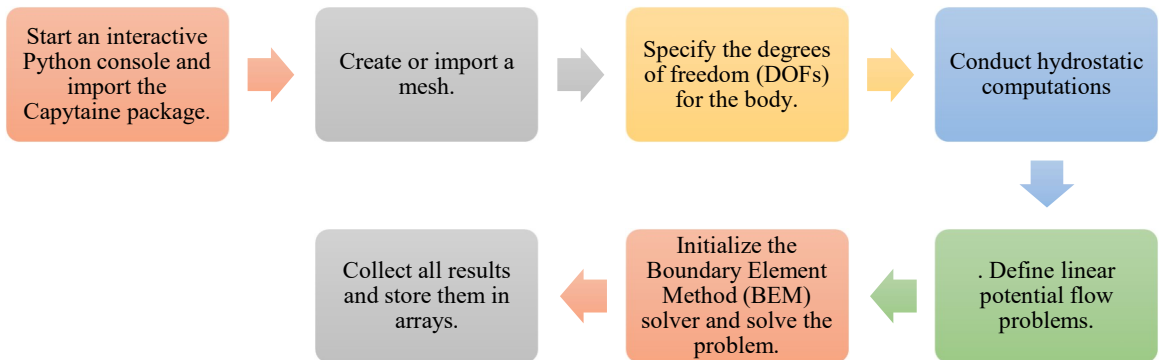


Figure 3.2: Capytaine process chart.

### 3.3 WEC-Sim Processing

The WEC-Sim numerical model, implemented in MATLAB using SIMULINK and SimMechanics toolboxes, follows a modular structure (Figure 3.1). WEC-Sim modules are categorized into three types:

- Pre-processing modules (blues) prepare user input data and perform non-time-independent calculations at the beginning of the simulation.
- Time domain modules (green) simulate specific components of the WEC system, solving the equation of motion.
- Post-processing modules (red) handle visualization and data analysis of simulation results.

Figure 3.1 illustrates the steps for creating a WEC-Sim simulation. At first, simple structural analysis is needed to be done to obtain the geometrical properties of the system, such as mass, moment of inertia, center of gravity, etc. Wave characteristics can be specified either as regular waves, i.e., specifying wave height and wave period or as wave spectrum. In the pre-processing module, WEC-Sim generates wave time-series data. A boundary element solver is used to generate frequency dependent hydrodynamic coefficients. In the present study, Capytaine is the boundary element method solver. The basic equations used to perform hydrodynamic diffraction analysis are outlined in Section 4.4. To perform time domain analysis, a multi-body dynamics WEC model is created using Simulink. Time domain modules simulate specific device components. System dynamic response is obtained by solving Cummins equation numerically using the 4<sup>th</sup> order Runge-Kutta algorithm. Post-processing modules are responsible for result visualization and analysis.

### 3.4 Equation of motion in time domain

For floating bodies, such as the point absorber wave energy converter (WEC) studied in this research, the hydrodynamic forces are determined using a common approach based on linear wave theory, which considers the waves as a combination of incident, radiated, and diffracted wave components. The dynamic response of the system is then computed by solving the equations of motion in the time domain for the WEC system. An overview of this approach is outlined below.

In the time domain, the equation of motion of a floating body about its center of gravity can be expressed as (Yu, Lawson, et al., 2014) -

$$m\ddot{x}(t) = F_{exc}(t) + F_{rad}(t) + F_{hs}(t) + F_{PTO}(t) + F_m(t) + F_v(t) \quad 3.1$$

where,  $m$  = mass matrix,  $\ddot{x}$  = device acceleration,  $F_{exc}$  = wave excitation force,  $F_{rad}$  = wave radiation force,  $F_{hs}$  = hydrostatic restoring force,  $F_{PTO}$  = power take-off (PTO) force,  $F_m$  = mooring force, and  $F_v$  = viscous damping force. It should be noted, that while the above equation includes the variable  $\ddot{x}$  as the device acceleration, this is really a 3D vector including accelerations in the  $x$ ,  $y$ , and  $z$  directions.

The inviscid hydrodynamic forces, such as  $F_{exc}$  and  $F_{rad}$ , are calculated by modeling linear coefficients obtained through a potential flow boundary element method (BEM) solver (i.e. Capytaine). The resistive force on the body due to wave radiation,  $F_{rad}$ , can then be calculated using the following equation,

$$F_{rad}(t) = -A^\infty \ddot{x}(t) - \int_{-\infty}^t K(t - \tau) \dot{x}(\tau) d\tau \quad 3.2$$

where  $A^\infty$  is the added mass matrix when the frequency is close to infinity (Ricci, 2016).  $A^\infty$  can be obtained using the potential flow BEM solver. The second term in Equation 3.2 is called a convolution integral, where,  $K$  is called the radiation impulse response

function (RIRF), also known as a memory function. The convolution integral represents the memory effect on the WEC dynamics.

Radiated waves generate from the body's motions, but they continue to propagate even after the motions cease. To account for the effects of these forces resulting from past motions, radiated forces are modeled using the convolution of the RIRF. Once the frequency-dependent radiation damping coefficient,  $B(\omega)$ , and added mass coefficient,  $A(\omega)$ , are obtained, RIRF can be calculated using either of the two following equations:

Equation 3.3 is used to calculate RIRF usually because it is less prone to

$$K(t) = \frac{2}{\pi} \int_0^{\infty} B(\omega) \cos \omega t d\omega \quad 3.3$$

$$K(t) = -\frac{2}{\pi} \int_0^{\infty} \omega \bar{A}(\omega) \sin \omega t d\omega, [\bar{A}(\omega) = A(\omega) - A^{\infty}] \quad 3.4$$

numerical inaccuracies (Ricci, 2016). After calculating  $K(t)$  from Equation 3.3, the added mass coefficient at infinite frequency which gives the device's instantaneous response to acceleration, can also be computed using the following equation (Ricci, 2016):

$$A^{\infty} = \frac{1}{N} \sum_{n=1}^N (A(\omega_n)) + \frac{1}{\omega_n} \int_0^{\infty} K(t) \sin \omega_n t dt \quad 3.5$$

Substituting Equation 3.2 in Equation 3.1, it can be written as-

$$m\ddot{x}(t) = F_{exc}(t) - A^{\infty} \ddot{x}(t) - \int_{-\infty}^t K(t - \tau) \dot{x}(\tau) d\tau + F_{hs}(t) + F_{PTO}(t) + F_m(t) + F_v(t) \quad 3.6$$

Equation 4.6 is called the Cummins' Equation in six degrees of freedom (DOF) to determine the motion and forces on a WEC device (Cummins, 1962).

In the time domain model, hydrostatic forces can be represented as a simple linear function of body displacement,  $x(t)$ , when the motion amplitudes are small. However, for larger amplitudes, nonlinear representations of hydrostatic forces are used. Additionally,

numerical integration of hydrostatic pressure over the wetted surface of the body is performed for various displacements. The excitation force in the time domain can be computed using its frequency-dependent expressions, obtained by convolving the wave surface elevation with the impulse response function (Ricci, 2016).

$$F_{exc}(t) = \int_{-\infty}^{+\infty} \eta(\tau) f_{exc}(t - \tau) d\tau \quad 3.7$$

where,  $\eta$  = wave elevation, and  $f_{exc}(t)$  = impulse response function (IRF) =  $\frac{1}{2\pi} \int_{-\infty}^{+\infty} F_{exc}(\omega, \theta) e^{i\omega t} d\omega$ .  $F_{exc}(\omega)$  represents the frequency-dependent excitation force component obtained from the BEM solver,  $\omega$  represents wave frequency, and  $\theta$  denotes the wave direction. This convolution integral form of excitation force is utilized for modeling user-defined wave elevation cases.

For irregular waves with wave spectrum  $S(\omega)$ , it can be computed using the following equation,

$$F_{exc}(t) = \Re [ R_f(t) \sum_{j=1}^N F_{exc}(\omega, \theta) e^{i(\omega t + \varphi)} \sqrt{2S(\omega)} d\omega ] \quad 3.8$$

Here,  $\varphi$  is the randomized phase angle, and  $N$  is the number of frequency bands selected to discretize the wave spectrum. NDBC buoy observations provide spectral wave density data in 47 unevenly spaced bins. However, WEC-Sim requires input with approximately 1000 evenly spaced frequency bins for user defined spectra.

The simplest representation of the Power Take-Off (PTO) force involves considering a linear force that opposes the motion of the WEC. This force consists of two terms: one is proportional to the velocity of the WEC, and the other is proportional to the displacement of the WEC, as shown in Equation 3.9 (Pecher & Kofoed, 2017).

$$F_{PTO} = -D\dot{x}(t) - kx(t) \quad 3.9$$

The first term in Equation 3.9 corresponds to the resistive force component, where  $D$  represents the damping coefficient. This term accounts for a resistive or dissipative effect and is related to the WEC's ability to extract wave energy. The second term in Equation 3.9 represents a reactive force that is proportional to the displacement, where  $k$  is the spring coefficient. This term reflects a reactive effect associated with the energy exchange between the PTO and the moving part of the WEC. The reactive power is connected to the difference between the maximum values of kinetic and potential energy. However, it is important to note that the reactive force component does not contribute to the time-averaged absorbed power since the time-averaged reactive power is zero (Pecher & Kofoed, 2017).

The mooring load,  $F_m$ , is represented by using a linear quasi-static mooring stiffness. When employing a linear quasi-static mooring stiffness, the mooring load can be determined using the following equation,

$$F_m = -K_m x - C_m \dot{x} \tag{3.10}$$

Here,  $K_m$  and  $C_m$  represent the stiffness and damping matrices for the mooring system, while  $x$  and  $\dot{x}$  denote the displacement and velocity of the body, respectively (WEC-Sim, 2022). The quasi-static catenary modeling approach calculates the tension in a catenary mooring line by considering fairlead and anchor positions. It involves using nonlinear quasi-static catenary line equations in the wave-to-wire model to determine the tension at the fairleads during each time step. While this method is simple and computationally efficient, it is limited to small motions around the mean position (Pecher & Kofoed, 2017). When a body is submerged in a liquid, it encounters an upward buoyant force equivalent to the weight of the displaced liquid, following Archimedes' principle. The hydrostatic force,  $F_{hs}$ , emerges from the disparity between this upward force and the body's weight, resulting in buoyancy variations and consequent changes in the hydrostatic force caused by the body's oscillatory motion. Linear theory assumes that body motions have small amplitudes, which aligns with the behavior of WECs during

typical operational conditions. WECs tend to have small amplitude motions to avoid dominant dissipative viscous effects, which could limit motion and reduce device efficiency. Therefore, the hydrostatic force, represented by  $F_{hs}$ , is commonly modeled in wave-to-wire models as a function proportional to the body displacement, and the proportionality coefficient is known as the hydrostatic coefficient (Pecher & Kofoed, 2017),

$$F_{hs}(t) = G_m x(t) \tag{3.11}$$

where,  $G_m$  is the hydrostatic coefficient, and  $x$  represents the displacement vector.

For small amplitude heaving body oscillations, the variation in buoyancy force can be simply expressed as shown in Equation 3.12 (Pecher & Kofoed, 2017).

$$F_{hs}(t) = \rho g A x(t) \tag{3.12}$$

Here,  $\rho$  denotes the water density,  $g$  is the gravitational acceleration,  $A$  is the cross-sectional area of the body in undisturbed conditions, and  $x$  is the vertical displacement of the body. The change in the volume of water displaced is equal to the variation in the body's submerged volume, given by  $Ax$  (Pecher & Kofoed, 2017).

Viscous damping forces,  $F_v$ , are the combination of linear damping and quadratic drag forces, defined as,

$$\begin{aligned} F_v &= -C_v \dot{x} - \frac{C_d \rho A_d}{2} \dot{x} |\dot{x}| \\ &= -C_v \dot{x} - C_D \dot{x} |\dot{x}| \end{aligned} \tag{3.13}$$

In Equation 3.13,  $C_v$  represents the linear (viscous) damping coefficient,  $C_d$  denotes the quadratic drag coefficient,  $\rho$  signifies the fluid density, and  $A_d$  stands for the characteristic area used in drag calculation. Alternatively,  $C_D$  can be defined directly (WEC-Sim, 2022).

## Chapter 4 – Modelling and Simulation

### 4.1 Scaled model geometry characteristics

As mentioned in Section 2.6, the reference model for this project has been chosen as RM3. For this project, Froude scaling was used to generate the scaling factor and details for the RM3 scaled model. Froude scaling is a crucial method for scaling wave energy converters (WECs) as it ensures that the hydrodynamic behavior and performance of scaled models accurately represent those of full-scale devices. The device geometry and specifications are as follows:

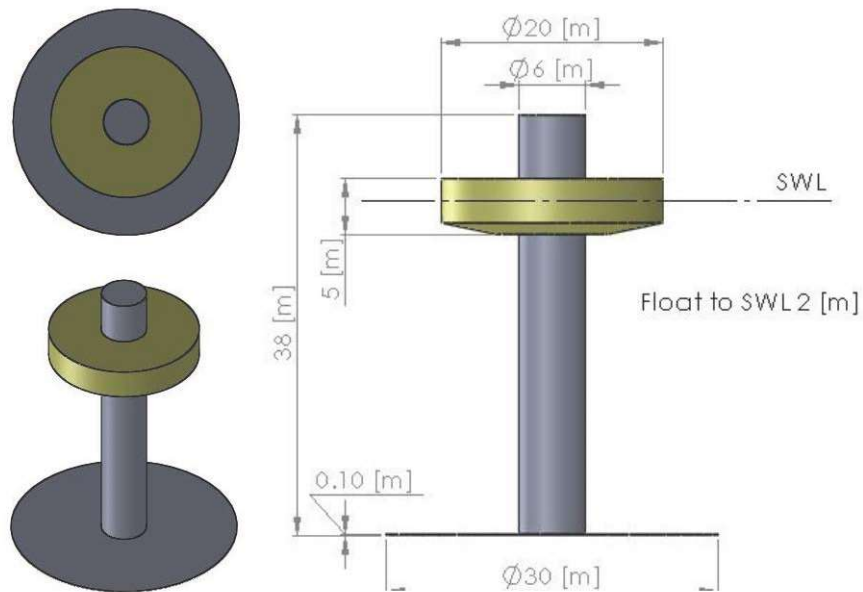


Figure 4.1: Full-scale Reference Model 3 (RM3) modified by the WEC-Sim team (*WEC-Sim*, 2022). The yellow cylindrical feature near the top is the float. The other component of the RM3 WEC is called the spar.

Table 4.1:: Mass of the two bodies of the RM3 reference model (*WEC-Sim*, 2022)

Body	Mass (In metric tons = 1000 kg)
Float	727.01
Spar	878.30

Table 4.2: RM3 reference model specification (*WEC-Sim*, 2022).

Body	Direction	Center of Gravity (m)	Moment of Inertia Tensor (kg.m <sup>2</sup> )		
Float	x	0	20,907,301	0	0
	y	0	0	21,306,091	0
	z	-0.72	0	0	37,085,481
Spar	x	0	94,419,615	0	0
	y	0	0	94,407,091	0
	z	-21.29	0	0	28,542,225

The model CAD files have been collected from the WEC-Sim GitHub repository. After collecting the CAD files, the two parts of the body have been scaled using the Froude scaling method, as mentioned in Section 2.6. As the scaling factor was 1/3<sup>rd</sup> of the original model, the scaled specifications of the model are as follows,

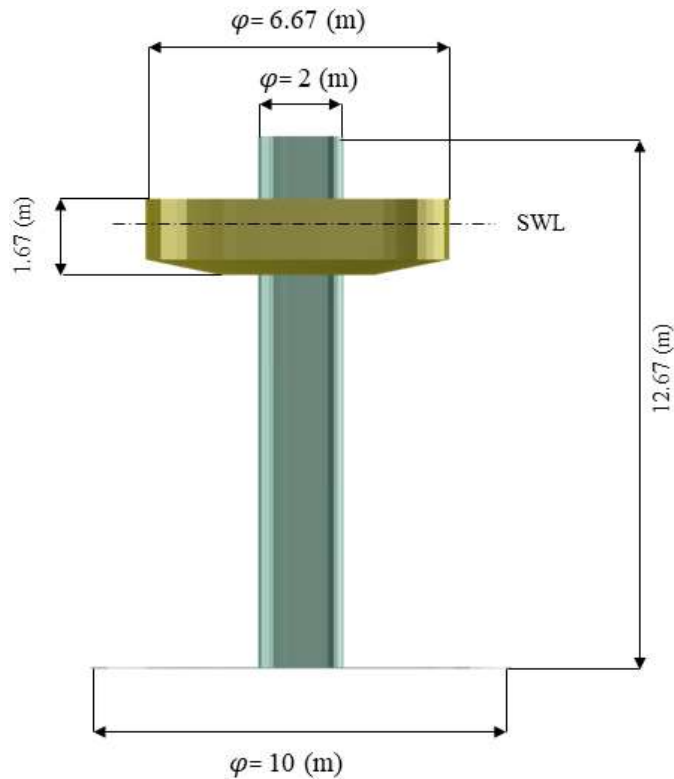


Figure 4.2: CAD model and dimensions of the scaled RM3 float and spar.

Table 4.3: Mass of the two separate bodies of the scaled RM3 reference model.

Body	Mass (In metric tons = 1000 kg)
Float	26.926
Spar	32.530

Table 4.4: Specifications of the scaled RM3 model.

Body	Direction	Center of Gravity (m)	Moment of Inertia Tensor (kgm <sup>2</sup> )		
			I <sub>xx</sub>	I <sub>yy</sub>	I <sub>zz</sub>
Float	x	0	86,038	0	0
	y	0	0	87,679	0
	z	-0.24	0	0	152,615
Spar	x	0	388,558	0	0
	y	0	0	388,507	0
	z	-7.097	0	0	117,458

## 4.2 3D diffraction and radiation analysis methodology using Capytaine

In this study, Capytaine has been employed as the BEM solver to calculate the excitation force ( $F_{exc}$ ), added mass matrix ( $A(\omega)$ ), damping matrix ( $F_{rad}$ ), and hydrostatic ( $F_{hs}$ ) coefficient of the body. First, the mesh is imported into Capytaine using Meshmagick and sorted as a Mesh object. To analyze diffraction or radiation problems in Capytaine, the next step required defining degrees of freedom (DOFs) of the body. This is achieved by creating a FloatingBody object. The rotation center is used to define the rotation degrees of freedom, while the center of mass parameter is used for certain hydrostatic properties. The degrees of freedom are stored in the DOFs dictionary within the FloatingBody object.

Capytaine provides direct functionality for hydrostatic computations, allowing users to obtain various parameters for a given FloatingBody. These parameters include volume, wet surface area, waterplane area, center of buoyancy, metacentric radius and height, hydrostatic stiffness, and inertia matrix. To calculate these hydrostatic parameters, Capytaine offers separate methods for each parameter. Some of these methods require the user to define the center of mass of the body. After the hydrostatic stiffness and inertia

calculations, Capytaine returns a 6 x 6 2D hydrostatic stiffness matrix and a 6 x 6 2D inertia matrix. These matrices capture the hydrostatic characteristics of the FloatingBody.

After that, the radiation and diffraction problem was defined. The wave frequency ranged between 0.035 Hz to 5.2 Hz, with total of 50 bins. The device is mostly symmetric about the Z-axis, so wave direction is not an important criterion to be considered. The wave heading angle was considered as 0 degrees. The water depth is infinite, gravitational acceleration is  $g = 9.8 \text{ ms}^{-2}$ , and the water density has been chosen as  $\rho = 1000 \text{ kgm}^{-3}$  to represent Lake Superior's freshwater environment (Babarit & Delhommeau, 2015), (Ancellin & Dias, 2019).

Finally, the BEM solver is initialized. Since the radiation problem is solved, the added mass and radiation damping can be accessed now. The solver also calculates the Froude-Krylov forces and stores them in a NetCDF file which includes the values of the different variables.

### **4.3 Simulink PTO**

Upon finalizing all input parameters, including wave spectrum, buoy dimensions, mass properties, hydrodynamic data, and power take-off systems, a Simulink model is constructed utilizing the WEC-Sim library. Figure 4.3 illustrates the model, with the float and spar represented by the rigid body block, connected to the translational PTO actuation force system that constrains the float's movement solely in the vertical direction. Then, a subsystem called PTO-Sim is created, which has an input and output of response and force, respectively. The PTO-Sim includes hydraulic cylinder, rectifying valve, and accumulator blocks for the hydraulic block and electric generator equivalent circuit in the electric generator block. The global reference frame in the bottom is used to mimic the seabed. Subsequently, simulation parameters, body properties, wave properties, and PTO parameters, are defined in the WEC-Sim input file (Appendix A).

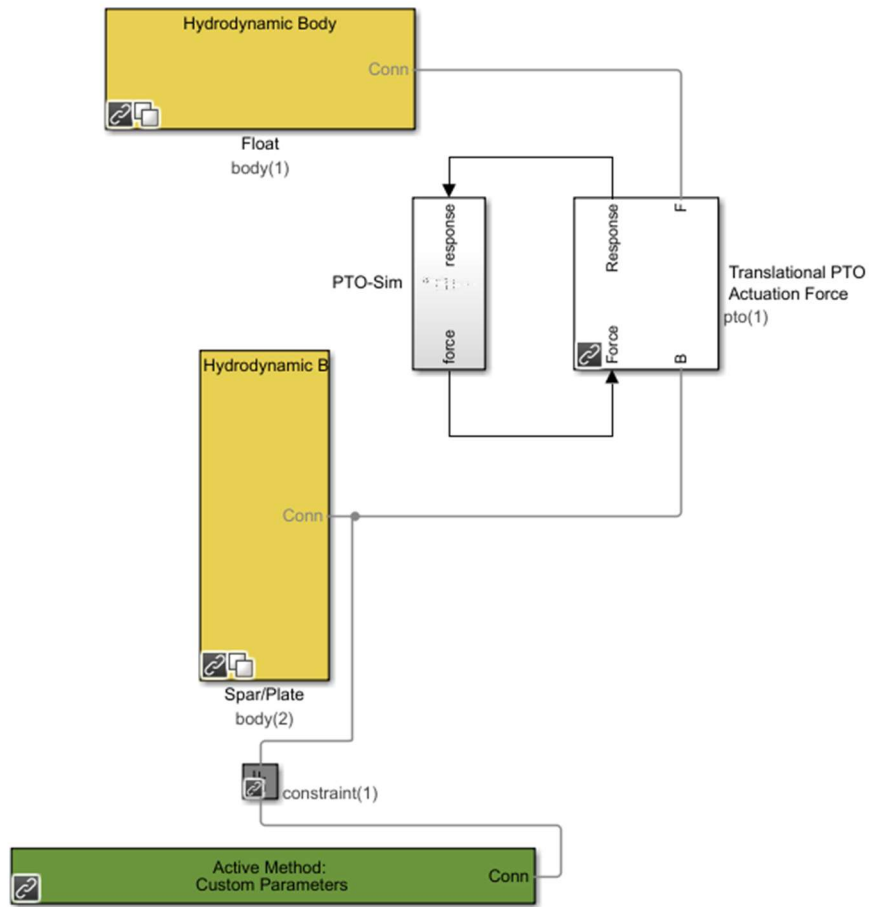


Figure 4.3: Simulink model for the hydraulic PTO used during this study of the RM3.

#### 4.4 Pre-processing in WEC-Sim using BEMIO

Following the computation of hydrodynamic coefficients using Capytaine, the subsequent stage involves creating a HDF5 file to store all nondimensionalized hydrodynamic coefficients. This is accomplished by running a ‘Boundary Element Method Input/Output (BEMIO)’ code, which converts the hydrodynamic coefficient data stored in the NETCDF file into the HDF5 (.h5) file format. After running BEMIO code, WEC-Sim calculates the following:

**Normalized Coefficients:** WEC-Sim calculates the normalized added mass coefficient, and normalized radiation damping coefficient using the following formulae (*WEC-Sim*, 2022):

$$\bar{A}(\omega) = \frac{A(\omega)}{\rho} \quad 4.1$$

$$\bar{B}(\omega) = \frac{B(\omega)}{\rho\omega} \quad 4.2$$

where  $\bar{A}$  and  $\bar{B}$  are the normalized added mass coefficient and normalized radiation damping coefficients, respectively, calculated for different wave frequencies. Here,  $\rho$  is the density of freshwater or seawater, and  $\omega$  is the wave frequency in rad/s.  $A(\omega)$  and  $B(\omega)$  are the added mass and radiation damping coefficients, respectively, obtained from BEM solver.

**Normalized Excitation Force:** Magnitudes of nondimensionalized wave excitation force,  $\bar{X}$  for one heading angle can be calculated by the following equation:

$$\bar{X} = \frac{X(\omega, \theta)}{\rho\omega} \quad 4.3$$

where,  $X(\omega, \theta)$  is the magnitude of excitation force for heave motion obtained from BEM solver (*WEC-Sim*, 2022).

**Normalized IRF of radiation and excitation forces:** Values of normalized radiation impulse response function (IRF)  $\bar{K}_r(t)$  and normalized excitation IRF  $\bar{K}_e(t)$  can be calculated using the following formulae:

$$\bar{K}_r(t) = \frac{2}{\pi} \int_0^\infty \frac{B(\omega)}{\rho} \cos(\omega t) d\omega \quad 4.4$$

$$\overline{K_e}(t) = \frac{1}{2\pi} \int_{-\infty}^{\infty} \frac{X(\omega, \theta) e^{i\omega t}}{\rho g} d\omega$$

4.5

Similar to the previous paragraphs, provide some description of the variables here in a sentence or two (*WEC-Sim*, 2022).

## Chapter 5 – Results and Discussion

Prior to modeling the dynamic response of the scaled RM3 point absorber WEC, a historical sea state analysis was performed to understand typical sea state conditions on Lake Superior. This initial step involved calculating the number of observations for various combinations of wave period and significant wave height from the historical data collected over 15 years (2008-2022) of NDBC buoy 45006, located in western Lake Superior. This data are presented in Table 5.1, providing insights into the occurrence frequency of different sea states. Observations over this 15 year period were binned into significant wave height bins of 0.5m from 0 to 5.5m, and across wave periods with bin widths of 1 second, ranging from 2 to 16 seconds. For this specific location at NDBC 45006, nearly all of the observations occurred with wave periods less than 10 seconds and below wave heights of 6 meters. The bold black box visible in Table 5.1 indicates the sea state conditions under which the RM3 scaled model was simulated using WEC-Sim.

Table 5.1: Observation counts for the NDBC 45006 sea states.

		Observation Counts - NOAA NDBC 45006 Sea States														
		Wave Period (s)														
		2.5	3.5	4.5	5.5	6.5	7.5	8.5	9.5	10.5	11.5	12.5	13.5	14.5	15.5	COUNT
Significant Wave Height (m)	0.25	2708	9846	2057	551	80	14	4	1				1	1		15263
	0.75	34	4045	6801	1352	429	72	2								12735
	1.25		10	1563	2107	371	183	8	1							4243
	1.75			29	1070	462	152	27	7							1747
	2.25				144	461	186	26	11							828
	2.75				4	80	114	28	11							237
	3.25					14	59	31	18							122
	3.75						24	19	15							58
	4.25						3	7	15	1						26
	4.75						1	3	5							9
	5.25							2	4							6
	5.75								3							3
6.25															0	
<b>TOTAL</b>															<b>35277</b>	

Next, using the results from Table 5.1 and the total number of observations, the joint probability distribution (JPD) was computed in Table 5.2, revealing the probability of specific wave period and significant wave height couples occurring together. For the location of NDBC 45006, the most common sea states were wave heights up to 1m with wave periods between 3-5 seconds, accounting for nearly 65.5% of all observations over the past 15 years. It is important to keep in mind that these observations occurred only when the buoy was deployed. Over the 15 years of data used, the buoy was typically deployed between April-October, so the statistics reported here account for about 50% of the year. According to modeling efforts and ongoing Great Lakes wave climate analysis, increased wave heights and longer wave periods are more common during the late fall, winter, and early spring seasons, typically when the NDBC buoy systems are not deployed. Compared to other low resource locations like Mediterranean sea, which has a significant wave height of 5-7m (Soukissian et al., 2017), in the Arabian Gulf, For a 100-year return period, the significant wave heights range from 3.0 to 4.5 meters across water depths ranging from 9 to 16 meters (Neelamani et al., 2007), and at Gulf of Mexico ranging from 1-2.5m ( collected from three NDBC buoys located in the central Gulf of Mexico near 26°N) (Hwang et al., 1997).

Table 5.2: Joint probability distribution (JPD) for the NDBC 45006 sea states using 15 years of observations (2008-2022).

		Joint Probability Distribution (JPD) - Probability of Occurrence of Sea States at NOAA NDBC 45006													
		Wave Period (s)													
		2.5	3.5	4.5	5.5	6.5	7.5	8.5	9.5	10.5	11.5	12.5	13.5	14.5	15.5
Significant Wave Height (m)	0.25	7.68%	27.91%	5.83%	1.56%	0.23%	0.04%	0.01%							
	0.75	0.10%	11.47%	19.28%	3.83%	1.22%	0.20%	0.01%							
	1.25			4.43%	5.97%	1.05%	0.52%	0.02%							
	1.75				3.03%	1.31%	0.43%	0.08%	0.02%						
	2.25					1.31%	0.53%	0.07%	0.03%						
	2.75					0.23%	0.32%	0.08%	0.03%						
	3.25					0.04%	0.17%	0.09%	0.05%						
	3.75						0.07%	0.05%	0.04%						
	4.25						0.01%	0.02%	0.04%						
	4.75							0.01%	0.01%						
	5.25							0.01%	0.01%						
	5.75								0.01%						
6.25															

Subsequently, WEC-Sim PTOsim simulations were performed for each non-zero JPD-valued wave period and significant wave height combination, indicated by the bold box outline bounding wave heights 0 to 5 meters and wave periods 2 to 10 seconds in Table 5.2. The simulations were executed with a ramp time of 100s and a time step size of 0.01s, spanning a total simulation time of 400s. It was observed that despite the ramp time being set to 100s, stability was achieved after around 200s. Figure 5.1 shows the ramp up needed for the motor to get to a steady state.

Following the PTOsim simulations, essential plots were generated, including motor speed, PTO force, piston pressure and power output, for the occurrence with the second highest JPD value of 19.28% (4.5s and 0.75m). These plots are illustrated in Figure 5.1, and Figure 5.3-Figure 5.6, capturing key performance metrics.

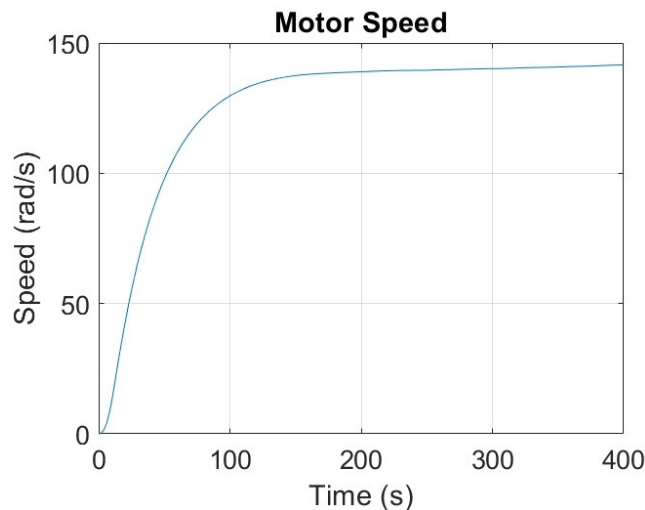


Figure 5.1 Plot illustrating the ramp up time for the hydraulic motor for a wave of 0.75m height with dominant wave period of 4.5s.

Figures 5.3 and 5.4 provide a detailed examination of the hydraulic Power Take-Off (PTO) system, focusing on the force generated and the pressures within the top and bottom piston pumps. These specific visuals offer valuable insights into the complex dynamics of the hydraulic components integral to the wave energy converter (WEC)

system. In Figure 5.2, we observe the presence of check valves strategically positioned between the pistons and the accumulators. These check valves play a pivotal role within the hydraulic system. When the velocity of the piston reaches zero, a distinct hydraulic scenario emerges. At this juncture, the pressure on the piston side of the system is insufficient to trigger the opening of the check valves. Consequently, the check valves remain in a closed state. Their design dictates that they only open under precise circumstances.

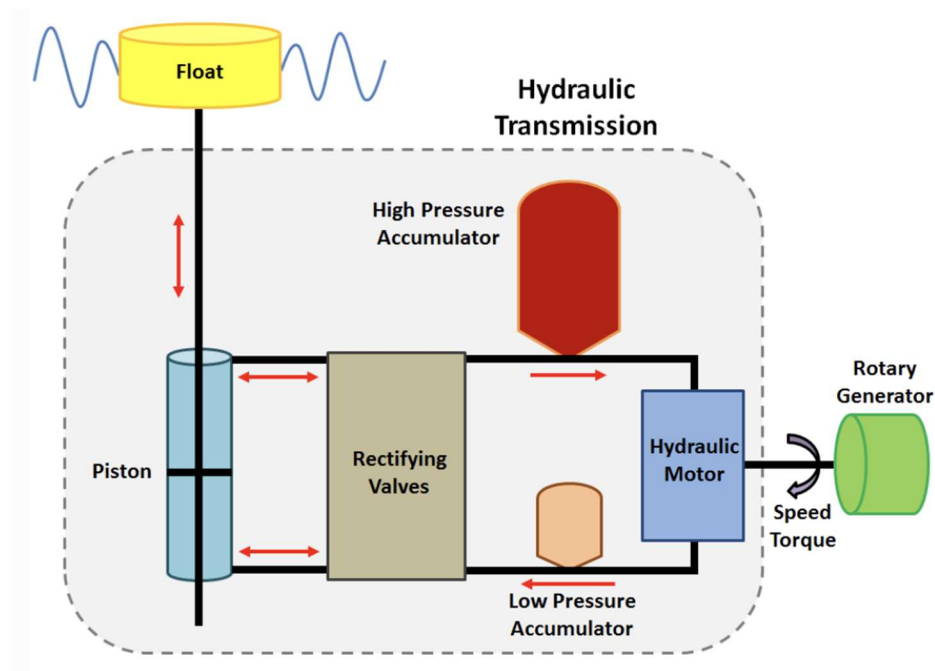


Figure 5.2: Artist's representation of the hydraulic PTO system (*WEC-Sim*, 2022).

There are two critical scenarios that lead to the opening of these check valves. First, when the pressure in the top piston exceeds the predefined threshold of the high-pressure accumulator, the check valve responds by opening. Second, if the pressure in the bottom piston falls below the predetermined threshold for the low-pressure accumulator, the check valve also opens.

A noteworthy aspect of this hydraulic configuration is the emergence of a spring-like effect due to the compressibility of the modeled fluid and the behavior of the check valves. This unique phenomenon results from the interaction between pressure differentials, valve dynamics, and the compressibility of the fluid. As a consequence, the pressure on the piston side of the system oscillates and gradually decays. This oscillatory behavior continues until an adequate excitation force is applied to the system, compelling the check valve to open. This hydraulic system therefore manifests an intrinsic latching control which is a discrete, highly non-linear, intrinsically sub-optimum control strategy (So et al., 2015).

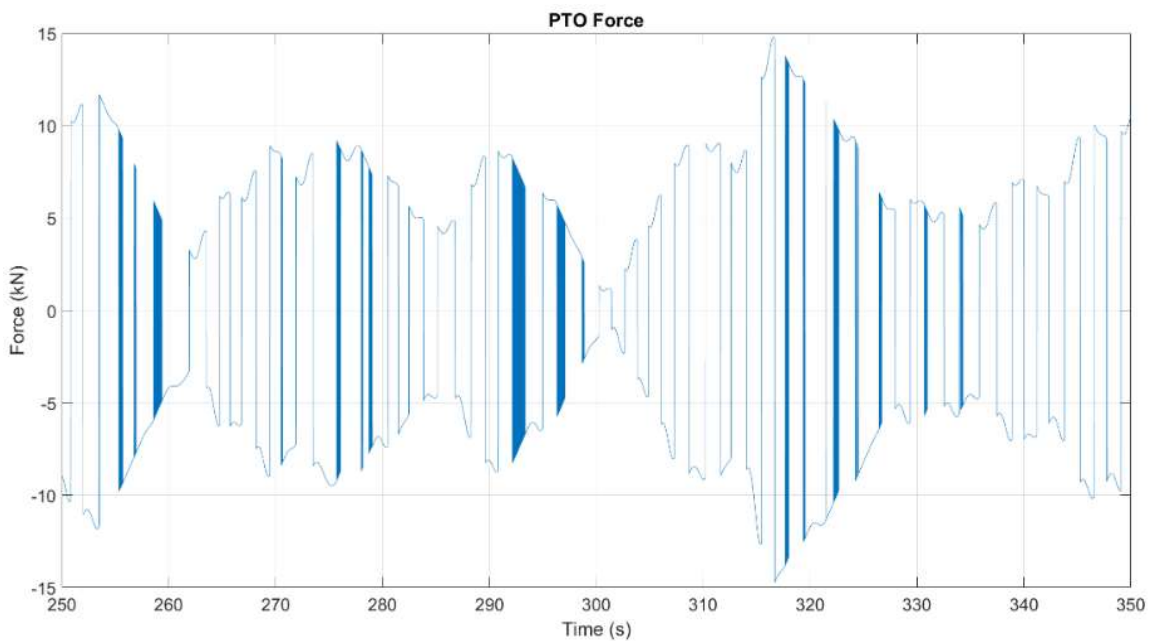


Figure 5.3: Zoomed view of the force generated the hydraulic PTO for a wave of 0.75m height with dominant wave period of 4.5s.

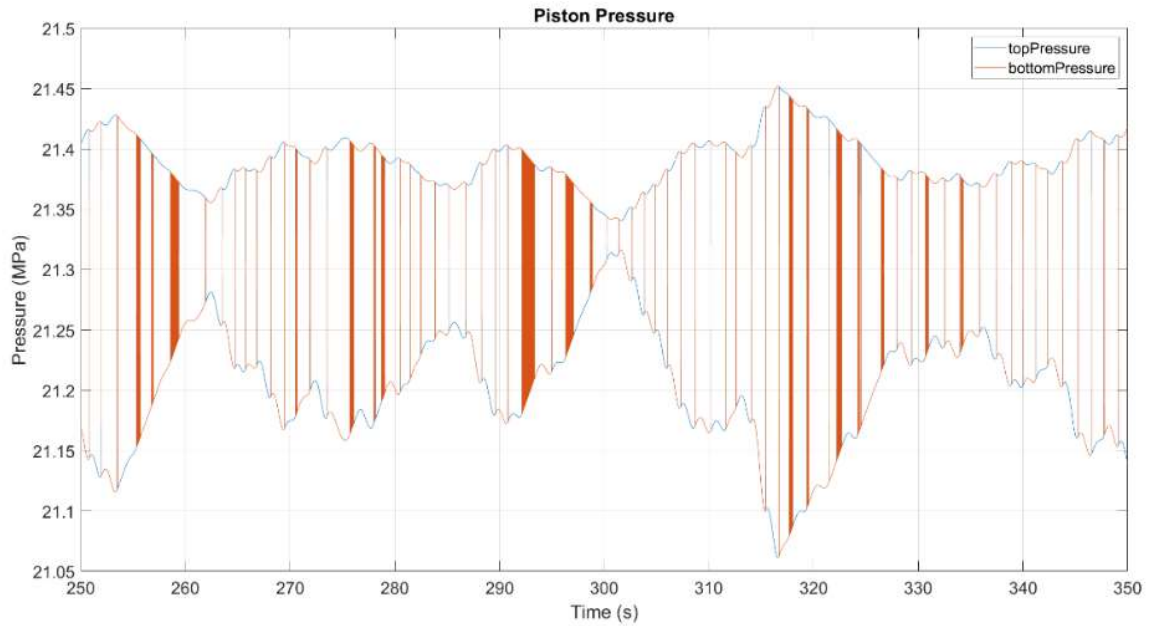


Figure 5.4: Top and bottom piston pump pressures for a wave of 0.75m height with dominant wave period of 4.5s.

In Figure 5.5, the full view and Figure 5.6, a detailed view of specific power metrics encompassing absorbed hydrodynamic power, mechanical power, and electrical power output during the interval of simulation time ranging from 250 seconds to 350 seconds has been shown. The generator employed in this study is characterized by a simplified rotational inertia model, complemented by a comprehensive lookup table that accounts for speed, torque, and efficiency attributes. The lookup table is established based on data extrapolated from a commonly used industrial induction generator.

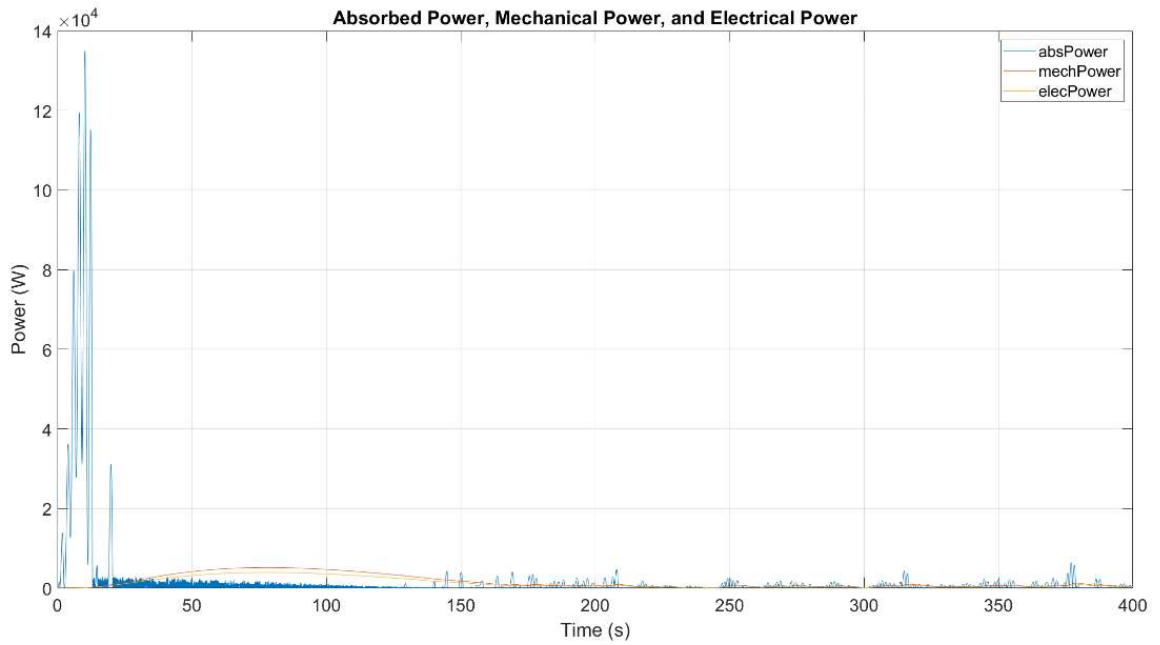


Figure 5.5: Full view of the plot showing the absorbed power, mechanical power and electrical power in kW.

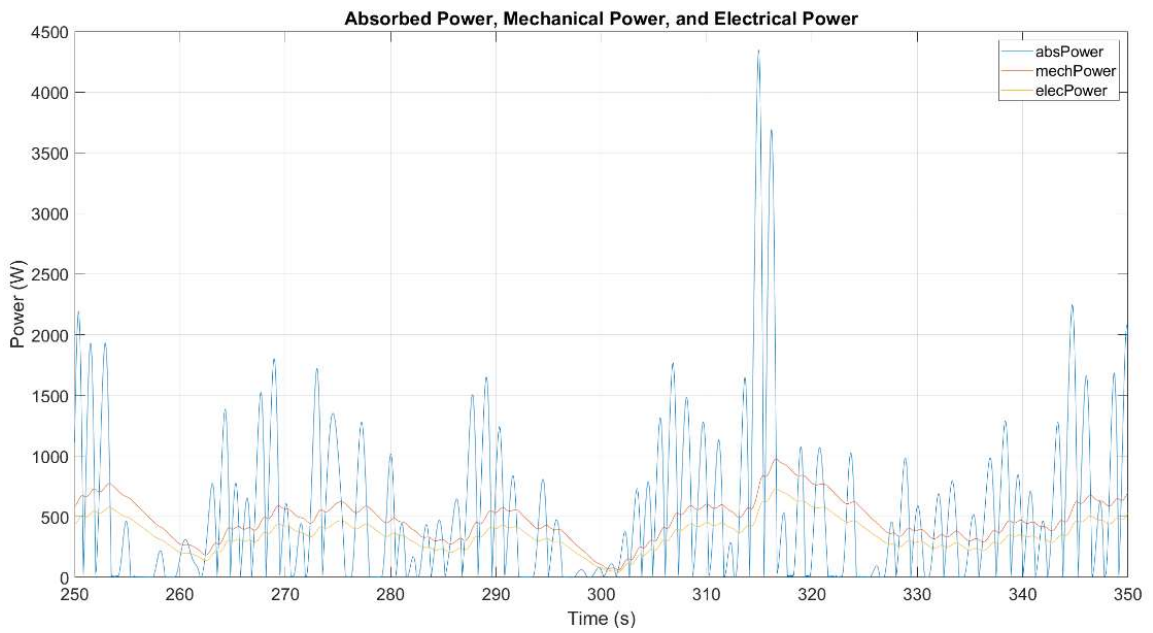


Figure 5.6: Detailed view of the plot showing the absorbed power, mechanical power and electrical power in kW.

The average values of absorbed, mechanical, and electrical power is observed to be 560 W, 505 W, and 379 W, respectively. Importantly, the efficiency in the conversion process from absorbed power to electrical power demonstrates a level of approximately 68%. Furthermore, the conversion efficiency from mechanical power to electrical power attains a magnitude of approximately 75%. This elucidates the effectiveness of the conversion mechanisms involved in harnessing wave energy and transforming it into usable electrical power, reinforcing the overall viability of the proposed wave energy converter system. Subsequently, the PTOsim simulations were run for a total of 54 different occurrences based on all non-zero JPD values, and the electrical power outputs were recorded and tabulated in Table 5.3. The annual average electrical power ( $P_{ae}$ ) was then derived from the collected data. Using Equation 5.1, the estimated annual energy production (AEP) was calculated in Table 6.4, with  $\beta$  representing the combined efficiencies related to transmission and WEC availability (Yu, Li, et al., 2014). For this particular case,  $\beta=1$  was reasonably estimated. The AEP provides an estimate of the annual power output expected from this modeled WEC. This comprehensive analysis contributes to understanding the potential energy production capabilities of the WEC under various sea states and operational conditions.

$$AEP = P_{ae} \times \beta \times 8760$$

5.1

Table 5.3: Electric power matrix (in kW) for the modeled RM3 WEC.

		Electric Power Matrix-KW													
		Wave Period (s)													
		2.5	3.5	4.5	5.5	6.5	7.5	8.5	9.5	10.5	11.5	12.5	13.5	14.5	15.5
Significant Wave Height (m)	0.25	0.10	0.09	0.02	0.02	0.01	0.01								
	0.75	0.76	0.43	0.38	0.24	0.17	0.22	0.24	0.20						
	1.25		1.23	0.89	0.82	0.99	1.28	1.49	1.37						
	1.75			1.98	2.98	2.52	2.89	3.28	3.36						
	2.25				5.26	6.27	4.97	5.32	5.57						
	2.75				7.87	12.45	10.35	7.39	8.35						
	3.25					16.27	20.91	14.22	12.39						
	3.75						29.76	23.41	16.45						
	4.25						18.27	29.65	23.77						
	4.75							29.02	30.24						
	5.25							21.58	34.56						
	5.75								24.98						
6.25															

Table 5.4: Annual energy production (AEP) (MWh) for the modeled WEC. Sea states with blank boxes were not simulated in WEC-Sim.

		Annual Averaged Electrical Power ( $P_{ac}$ ) (kW)																
		Wave Period (s)																
		2.5	3.5	4.5	5.5	6.5	7.5	8.5	9.5	10.5	11.5	12.5	13.5	14.5	15.5	Total		
Significant Wave Height (m)	0.25	0.007	0.024	0.001												0.033		
	0.75	0.001	0.049	0.073	0.009	0.002										0.135		
	1.25			0.039	0.049	0.010	0.007									0.107		
	1.75			0.002	0.090	0.033	0.012	0.003	0.001							0.141		
	2.25				0.021	0.082	0.026	0.004	0.002							0.135		
	2.75				0.001	0.028	0.033	0.006	0.003							0.071		
	3.25					0.006	0.035	0.012	0.006							0.060		
	3.75						0.020	0.013	0.007							0.040		
	4.25						0.002	0.006	0.010							0.018		
	4.75							0.002	0.004							0.007		
	5.25								0.001	0.004						0.005		
	5.75															0.002		
	6.25															0.000		
																$P_{ac}$	0.753	kW
																Beta	1.000	
																AEP (No Loss)	6597.427	kWh
																AEP (With Beta)	6597.427	kWh
																AEP (With Beta)	6.597	MWh

This study highlights the significant potential of this WEC in Lake Superior as a valuable contributor to the blue economy and marine renewable energy sector. With an annual average electrical power output of approximately 753 W and an annual energy production of about 6.6 MWh, this WEC can play a pivotal role in enhancing the sustainability and efficiency of various oceanographic activities and aquaculture ventures.

The reliable and continuous power supply generated by the WEC can serve as a vital resource for remote oceanographic sensors and observation systems. This capability enables uninterrupted data collection, facilitating scientific research, environmental monitoring, and marine resource management. Accessibility to continuous power is paramount in addressing critical issues such as climate change, ecosystem dynamics, and oceanographic phenomena.

Furthermore, the WEC's capacity to recharge autonomous underwater vehicles (AUVs) and unmanned surface vessels (USVs) extends its utility beyond stationary applications. By providing the means to recharge these vehicles, the WEC enhances their operational capabilities for scientific research, exploration, and data gathering in marine environments. This advancement in autonomous vehicle technology is crucial for conducting in-depth studies and assessments in remote and challenging marine regions. The estimated power requirement for underwater vehicle recharging station can be between 66 kWh to 2.2 MWh depending on number of vehicles to give service to (LiVecchi et al., 2019).

Additionally, potential growth in aquaculture industries in Lake Superior and across the Great Lakes stands to benefit significantly from the power produced by this WEC. Small-scale aquaculture farms can utilize this energy source for essential functions such as water circulation, aeration, temperature control, and lighting systems. The adaptability of the WEC's power supply to diverse aquaculture requirements makes it a sustainable solution for supporting seafood production in the region. Power demands for aquaculture operations can vary widely, ranging from 4 to 715 megawatt-hours per year, depending on factors like farm size, location, and specific operational needs (LiVecchi et al., 2019).

In conclusion, the integration of small-scale wave energy converters in Lake Superior demonstrates not only their potential as a clean energy source but also their ability to catalyze advancements in marine research, autonomous vehicle technology, and aquaculture sustainability. These outcomes align with the broader objectives of the blue economy and marine renewable energy development, contributing to both economic growth and environmental stewardship in the region. As the transition towards renewable energy gains momentum, harnessing the power of Lake Superior's waves holds promise for a more sustainable and prosperous future.

## Chapter 6 – Conclusion

Renewable energy plays a pivotal role in mitigating the environmental consequences arising from the utilization of fossil fuels. However, substantial untapped potential exists in harnessing the inherent renewable energy resource within the Great Lakes region, with Lake Superior as a salient example. Despite its evident promise, the full exploration of this resource has been constrained by limited research efforts. This research represents an innovative endeavor aimed at systematically analyzing the practical capacity for electrical power generation derived from the prevalent wave energy spectrum encompassing Lake Superior. The simulation followed JONSWAP spectrum, covering significant wave heights of 0.25m to 6m and mean wave periods from 2s to 10s. The central objective of this research is to ascertain the optimal configuration for a heaving point absorber wave energy converter, designed to achieve maximal efficiency in capturing wave energy. The model has been reshaped to 1/3<sup>rd</sup> from an existing point absorber called RM3 developed by the Reference Model Project (RMP) project team. Through an exhaustive scrutiny, employing comprehensive time domain analysis of the devised wave energy converter, the study rigorously assesses point absorber's performance in generating power.

The calculated annual average electrical power output yielded by this wave energy converter stands at approximately 6.6 MWh. It is important to note that this figure only partially represents the actual power generation potential. The data collection period of most NDBC buoys spans around 6-7 months of the year (April-October) for 15 years, thereby missing critical data from intense storms occurring particularly during November-February. This omission likely significantly underestimates the energy output of the system because many large storms develop during these months when no surface water observation systems are deployed.

Integrating the energy produced by this wave energy converter with the buoys in Lake Superior holds the potential to efficiently power these structures. Moreover, the generated energy can serve to support offshore installations, encompassing exploration activities, vehicle recharging stations, and aquaculture farms. This strategic utilization of energy also presents an opportunity for evaluating the viability of incorporating the Great Lakes into the broader marine renewable energy assessment framework.

## Chapter 7 - Future Recommendations

A notable limitation of this project pertains to the inadequacy of comprehensive year-long data. To address this constraint, an alternative approach is to employ the WAVEWATCH III model. The WAVEWATCH III model, developed at the Marine Modeling and Analysis Branch (MMAB) of the Environmental Modeling Center (EMC) within the National Centers for Environmental Prediction (NCEP), builds upon prior models, specifically WAVEWATCH I and WAVEWATCH II, which were originally developed at Delft University of Technology and NASA Goddard Space Flight Center, respectively. This model employs a solution approach based on the random phase spectral action density balance equation for wavenumber-direction spectra. The model is versatile, accommodating applications in shallow waters, including the surf zone, and allows for wetting and drying of grid points. (Tolman et al., 2019). WAVEWATCH III is capable of simulating the propagation of ocean waves on a wide scale, factoring in elements like wind patterns, atmospheric pressure, and ocean currents. It delivers comprehensive insights into parameters like wave height, wave period, and wave direction at various oceanic locations. By leveraging the WAVEWATCH III's simulation capabilities, it becomes feasible to anticipate buoy data for the entirety of a year, thereby facilitating a close approximation of actual power output expectations.

A promising avenue for future exploration involves a comprehensive comparison of power outputs derived from distinct types of WECs. This comparative analysis holds potential for revealing insights into the optimal WEC design that aligns with the specific characteristics of the region under consideration. The study presented here only examined the dynamic response and power potential of a heaving point absorber WEC; however, the optimal design for wave climates similar to the Great Lakes might harness energy from wave surging motion, a combination of heave and surge, or some element of lift or drag driven devices operating in the orbital velocity zones of waves.

In addition, it is imperative to consider the optimization of the Power Take-Off (PTO) mechanism as a strategic endeavor. Enhancing the efficiency of the PTO system becomes pivotal in augmenting power absorption capacity, ultimately elevating the buoy's potential to harness available wave energy to a more substantial extent. This optimization process emerges as a valuable direction to enhance overall energy generation performance. The study presented here used default RM3 PTO characteristics, yet WEC-Sim users have control over PTO design, PTO component characteristics, and more. WECs operating in lower resource environments such as the Great Lakes will likely benefit from PTO designs tailored towards higher frequency, low amplitude waves.

## References

- [1] Ancellin, M., & Dias, F. (2019). Capytaine: A Python-based linear potential flow solver. *Journal of Open Source Software*, 4, 1341. <https://doi.org/10.21105/joss.01341>
- [2] AW-Energy. (2022a). *Waveroller*. <https://aw-energy.com/waveroller/>
- [3] Babarit, A., & Delhommeau, G. (2015). Theoretical and numerical aspects of the open source BEM solver NEMOH. *11th European Wave and Tidal Energy Conference (EWTEC2015)*.
- [4] Baca, E., Philip, R., Greene, D., & Battey, H. (2022). *Expert Elicitation for Wave Energy LCOE Futures* (NREL/TP-5700-82375, 1885577, MainId:83148; p. NREL/TP-5700-82375, 1885577, MainId:83148). <https://doi.org/10.2172/1885577>
- [5] Bojek, P. (2023a, July 11). *Technology deployment*. <https://www.iea.org/energy-system/renewables/wind>
- [6] Bojek, P. (2023b, July 11). *Technology deployment*. <https://www.iea.org/energy-system/renewables/solar-pv>
- [7] Bouhrim, H., & El Marjani, A. (2019). Wave Energy Assessment Along the Moroccan Atlantic Coast. *Journal of Marine Science and Application*, 18(2), 142–152. <https://doi.org/10.1007/s11804-018-00060-8>
- [8] *Capytaine, github repository*. (2021). [Computer software]. <https://github.com/capytaine/capytaine>
- [9] Cavagnaro, R. J., Copping, A. E., Green, R., Greene, D., Jenne, S., Rose, D., & Overhus, D. (2020). Powering the Blue Economy: Progress Exploring Marine Renewable Energy Integration With Ocean Observations. *Marine Technology Society Journal*, 54(6), 114–125. <https://doi.org/10.4031/MTSJ.54.6.11>
- [10] Coe, R. G., Ahn, S., Neary, V. S., Kobos, P. H., & Bacelli, G. (2021). Maybe less is more: Considering capacity factor, saturation, variability, and filtering effects of wave energy devices. *Applied Energy*, 291, 116763. <https://doi.org/10.1016/j.apenergy.2021.116763>
- [11] Conway, F. (2019). *Socio-Economic Perspectives of Wave Energy Development. Report by Oregon State University. Report for Oregon Wave Energy Trust (OWET)*. <https://tethys.pnnl.gov/publications/socio-economic-perspectives-wave-energy-development>
- [12] Cummins, W. E. (1962). *The Impulse Response Function and Ship Motions*. <https://dome.mit.edu/handle/1721.3/49049>
- [13] Eco Wave Power. (2020). *Wave Energy Made Possible*. EWPG Holding AB. [https://www.ecowavepower.com/wp-content/uploads/2021/05/EWPG\\_Holding\\_AB\\_AR\\_2020\\_eng.pdf](https://www.ecowavepower.com/wp-content/uploads/2021/05/EWPG_Holding_AB_AR_2020_eng.pdf)
- [14] Gobato, R., Gobato, A., & Fedrigo, D. (2015). *Study Pelamis system to capture energy of ocean wave*.

- [15] Heras-Saizarbitoria, I., Zamanillo, I., & Laskurain, I. (2013). Social acceptance of ocean wave energy: A case study of an OWC shoreline plant. *Renewable and Sustainable Energy Reviews*, 27, 515–524.  
<https://doi.org/10.1016/j.rser.2013.07.032>
- [16] Hildenbrand, K. (2014). *Wave-Energy Devices Might Affect the Natural Environment*.
- [17] Hwang, P., Jacobs, G., Thompson, E., & Wang, D. (1997). *A Three-Year Climatology of Waves and Winds in the Gulf of Mexico*. 22.
- [18] Ilyas, A., Kashif, S. A. R., Saqib, M. A., & Asad, M. M. (2014). Wave electrical energy systems: Implementation, challenges and environmental issues. *Renewable and Sustainable Energy Reviews*, 40, 260–268.  
<https://doi.org/10.1016/j.rser.2014.07.085>
- [19] Iphofen, R. (2022). *The UK Wave Power Project: Salter's Duck* (pp. 101–110).  
[https://doi.org/10.1007/978-3-031-15746-2\\_8](https://doi.org/10.1007/978-3-031-15746-2_8)
- [20] IRENA. (2021). *Renewable Power Generation Costs in 2021—Executive Summary*.
- [21] Kempener, R., & Neumann, F. (2014). Wave energy technology brief. *International Renewable Energy Agency (IRENA)*.
- [22] Khedkar, K., Nangia, N., Thirumalaisamy, R., & Bhalla, A. P. S. (2021). The inertial sea wave energy converter (ISWEC) technology: Device-physics, multiphase modeling and simulations. *Ocean Engineering*, 229, 108879.  
<https://doi.org/10.1016/j.oceaneng.2021.108879>
- [23] Kilcher, L., Fogarty, M., & Lawson, M. (2021). *Marine Energy in the United States: An Overview of Opportunities* (NREL/TP--5700-78773, 1766861, MainId:32690; p. NREL/TP--5700-78773, 1766861, MainId:32690).  
<https://doi.org/10.2172/1766861>
- [24] LiVecchi, A., Copping, A., Jenne, D., Gorton, A., Preus, R., Gill, G., Robichaud, R., Green, R., Geerlofs, S., & Gore, S. (2019). Powering the blue economy; exploring opportunities for marine renewable energy in maritime markets. *US Department of Energy, Office of Energy Efficiency and Renewable Energy. Washington, DC, 207*.
- [25] Marquis, L. (2010). *First Power Production figures from the Wave Star Roshage Wave Energy Converter*.
- [26] Masuda, Y. (1986). An Experience of Wave Power Generator through Tests and Improvement. In D. V. Evans & A. F. O. de Falcão (Eds.), *Hydrodynamics of Ocean Wave-Energy Utilization* (pp. 445–452). Springer Berlin Heidelberg.
- [27] Mitigation, C. C. (2011). IPCC special report on renewable energy sources and climate change mitigation. *Renewable Energy*, 20(11).
- [28] Mørk, G., Barstow, S., Kabuth, A., & Pontes, M. T. (2010). Assessing the global wave energy potential. In *Proceedings of the International Conference on Offshore Mechanics and Arctic Engineering—OMAE* (Vol. 3, pp. 447–454).  
<https://doi.org/10.1115/OMAE2010-20473>

- [29] National Renewable Energy Laboratory. (2022b). *Marine Energy Atlas*. <https://maps.nrel.gov/marine-energy-atlas/data-library/layers>
- [30] Neary, V. S., Previsic, M., Jepsen, R. A., Lawson, M. J., Yu, Y.-H., Copping, A. E., Fontaine, A. A., Hallett, K. C., & Murray, D. K. (2014). *Methodology for Design and Economic Analysis of Marine Energy Conversion (MEC) Technologies*.
- [31] Neelamani, S., Al-Salem, K., & Rakha, K. (2007). Extreme Waves in the Arabian Gulf. *Journal of Engineering Research*, 6.
- [32] Nguyen, H. P., Wang, C. M., Tay, Z. Y., & Luong, V. H. (2020). Wave energy converter and large floating platform integration: A review. *Ocean Engineering*, 213, 107768. <https://doi.org/10.1016/j.oceaneng.2020.107768>
- [33] O'Donncha, F., Zhang, Y., Chen, B., & James, S. C. (2018). An integrated framework that combines machine learning and numerical models to improve wave-condition forecasts. *Journal of Marine Systems*, 186, 29–36. <https://doi.org/10.1016/j.jmarsys.2018.05.006>
- [34] Pecher, A., & Kofoed, J. P. (Eds.). (2017). *Handbook of Ocean Wave Energy* (Vol. 7). Springer International Publishing. <https://doi.org/10.1007/978-3-319-39889-1>
- [35] Pérez-Collazo, C., & Iglesias, G. (2012, October). *Integration of Wave Energy Converters and Offshore Windmills*.
- [36] Poullikkas, A. (2014). Technology prospects of wave power systems. *Electronic Journal of Energy & Environment*.
- [37] Rahm, M. (2010). *Ocean Wave Energy: Underwater Substation System for Wave Energy Converters* [PhD Thesis].
- [38] Ricci, P. (2016). Time-Domain Models. In *Numerical Modelling of Wave Energy Converters* (pp. 31–66). Elsevier. <https://doi.org/10.1016/B978-0-12-803210-7.00003-7>
- [39] Ross, D. (1995). *Power from the Waves*. (No Title).
- [40] Rusu, E., & Soares, C. G. (2013). Coastal impact induced by a Pelamis wave farm operating in the Portuguese nearshore. *Renewable Energy*, 58, 34–49. <https://doi.org/10.1016/j.renene.2013.03.001>
- [41] Said, H. A., & Ringwood, J. V. (2021). Grid integration aspects of wave energy—Overview and perspectives. *IET Renewable Power Generation*, 15(14), 3045–3064. <https://doi.org/10.1049/rpg2.12179>
- [42] Sheng, W., Alcorn, R., & Lewis, T. (2014). Physical modelling of wave energy converters. *Ocean Engineering*, 84, 29–36. <https://doi.org/10.1016/j.oceaneng.2014.03.019>
- [43] So, R., Casey, S., Kanner, S., Simmons, A., & Brekken, T. K. A. (2015). PTO-Sim: Development of a power take off modeling tool for ocean wave energy conversion. *2015 IEEE Power & Energy Society General Meeting*, 1–5. <https://doi.org/10.1109/PESGM.2015.7285735>
- [44] Soukissian, T., Denaxa, D., Karathanasi, F., Prospathopoulos, A., Sarantakos, K., Iona, S., Georgantas, K., & Mavrakos, S. (2017). Marine Renewable Energy in the

- Mediterranean Sea: Status and Perspectives. *Energies*, 10.  
<https://doi.org/10.3390/en10101512>
- [45] Thorpe, T. W. (1999). *A Brief Review of Wave Energy*.
- [46] Tolman, H., Abdolali, A., Accensi, M., Alves, J.-H., Arduin, F., Babanin, A., Barbariol, F., Benetazzo, A., Bidlot, J., Booij, N., Boutin, G., Bunney, C., Campbell, T., Chalikov, D., Chawla, A., Cheng, S., Collins III, C., Filipot, J.-F., Flampouris, S., & Liang, Z. (2019). *User manual and system documentation of WAVEWATCH III (R) version 6.07*.
- [47] Wale, C., & Hill, M. (2018). *Using MATLAB & Simulink to Develop Renewable Energy Technologies*. <https://www.alternative-energy-tutorials.com/wave-energy/wave-energy-devices.html>
- [48] *WEC-Sim*. (2022). [Computer software]. <https://wec-sim.github.io/WEC-Sim/master/user/tutorials.html>
- [49] Whittaker, T., & Folley, M. (2012). Nearshore oscillating wave surge converters and the development of Oyster. *Philosophical Transactions. Series A, Mathematical, Physical, and Engineering Sciences*, 370, 345–364.  
<https://doi.org/10.1098/rsta.2011.0152>
- [50] Yu, Y.-H., Lawson, M., Ruehl, K., & Michelén Ströfer, C. (2014, January). *Development and Demonstration of the WEC-Sim Wave Energy Converter Simulation Tool*.
- [51] Yu, Y.-H., Li, Y., Hallett, K., & Hotimsky, C. (2014). Design and Analysis for a Floating Oscillating Surge Wave Energy Converter. *Volume 9B: Ocean Renewable Energy*, V09BT09A048. <https://doi.org/10.1115/OMAE2014-24511>

## APPENDIX A

This is the sample WEC-Sim code that has been used for this research. The code is available at <https://github.com/WEC-Sim/WEC-Sim>. In this code, the significant wave height, mean wave period, the wave spectrum type, the body mass of both bodies and moment of inertia of both bodies have been altered.

```
%% Simulation Data
simu = simulationClass();
simu.simMechanicsFile = 'RM3_Hydraulic_PTO.slx'; %Location of Simulink Model File with PTO-SIM
simu.startTime = 0;
simu.rampTime = 100;
simu.endTime=400;
simu.dt = 0.01;
simu.explorer = 'off'; % Turn SimMechanics Explorer (on/off)

%% Wave Information
% Irregular Waves using PM Spectrum
waves = waveClass('irregular');
waves.H =0.25;
waves.T = 3.5;
waves.spectrumType = 'JS';
waves.phaseSeed=1;
% waves.spectrumDataFile ='November_2016_interpolated.mat';

%% Body Data
% Float
body(1) = bodyClass('\rm3.h5');
body(1).geometryFile = '../geometry/float_scaled.stl';
body(1).mass = 26926;
body(1).momOfInertia = [86038 87679 152615];

% Spar/Plate
body(2) = bodyClass('\rm3.h5');
body(2).geometryFile = '../geometry/spar_scaled.stl';

body(2).mass = 32550;
body(2).momOfInertia = [388558 388507 117458];

%% PTO and Constraint Parameters
% Translational Constraint
constraint(1) = constraintClass('Constraint1');
constraint(1).loc = [0 0 0];

% Translational PTO
pto(1) = ptoClass('PTO1'); % Create PTO Variable and Set PTO Name
pto(1).k = 0; % PTO Stiffness [N/m]
pto(1).c = 0; % PTO Damping [N/(m/s)]
pto(1).loc = [0 0 0]; % PTO Location [m]
```

## APPENDIX B

The full plotting of the piston pump pressure and the pressure exerted by the hydraulic PTO has been added here. The detailed view has been added at Chapter 5 for better visualization.

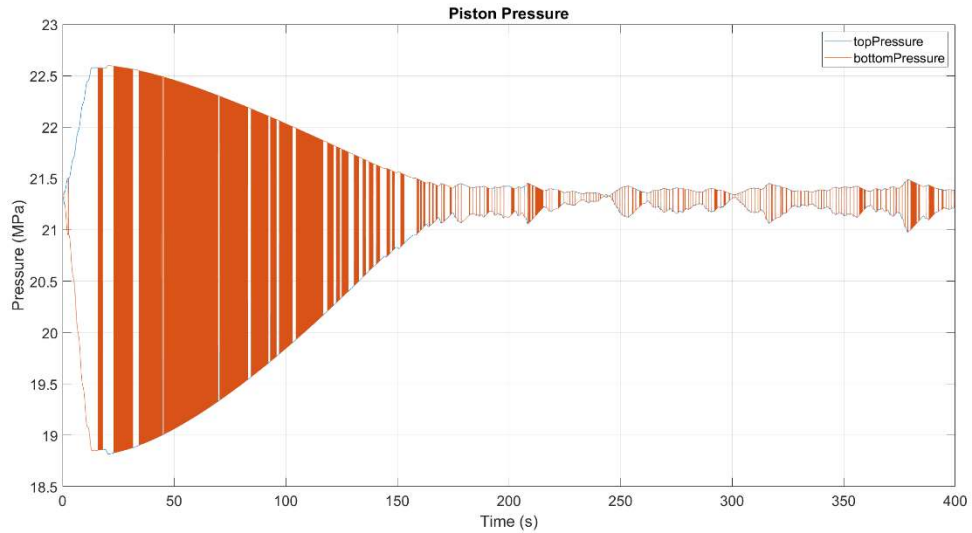


Figure A.1: Top and bottom piston pump pressures.

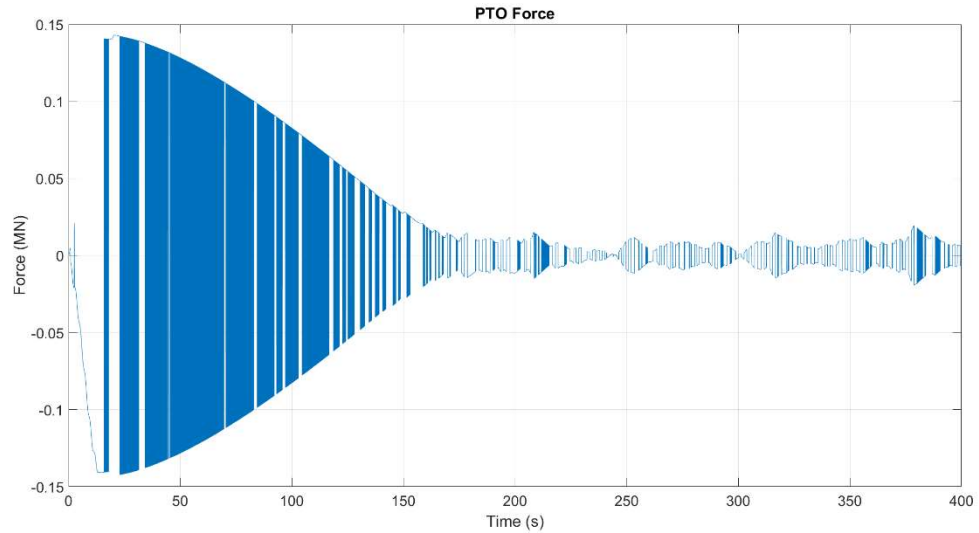


Figure A.2: Force applied by the PTO of the scale RM3 WEC.